

Protonation and Complexation Properties of Polyaromatic Terdentate Six-Membered Chelate Ligands

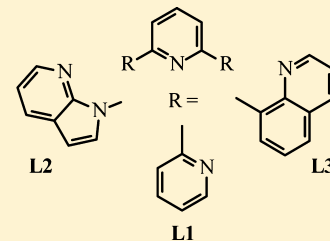
Thi Nhu Y Hoang,[†] Timothée Lathion,[†] Laure Guénée,[‡] Emmanuel Terazzi,[†] and Claude Piguet^{*,†}

[†]Department of Inorganic, Analytical and Applied Chemistry, University of Geneva, 30 quai E. Ansermet, CH-1211 Geneva 4, Switzerland

[‡]Laboratory of Crystallography, University of Geneva, 24 quai E. Ansermet, CH-1211 Geneva 4, Switzerland

Supporting Information

ABSTRACT: The successive protonation steps occurring in 2,2';6',2"-terpyridine (**L1**) are characterized by a strong affinity for the first entering proton ($\Delta G_{\text{connect}}^{\text{H,L1}} = -17 \text{ kJ/mol}$) followed by allosteric anticooperativity ($\Delta E_{\text{interaction}}^{\text{H,H,L1}} = 6 \text{ kJ/mol}$), a behavior mirrored by 2,6-bis(azaindolyl)pyridine (**L2**) despite the extension of the chelate ring size from five members (**L1**) to six members (**L2**; $\Delta G_{\text{connect}}^{\text{H,L2}} = -28 \text{ kJ/mol}$ and $\Delta E_{\text{interaction}}^{\text{H,H,L2}} = 7 \text{ kJ/mol}$). On the contrary, 2,6-bis(8-quinolinyl)pyridine (**L3**) is less eager for the initial protonation ($\Delta G_{\text{connect}}^{\text{H,L3}} = -10 \text{ kJ/mol}$), but the fixation of a second proton in $[\text{H}_2\text{L3}]^{2+}$ is driven to completion by positive cooperativity ($\Delta E_{\text{interaction}}^{\text{H,H,L3}} = -5 \text{ kJ/mol}$). Because of its unusual ability to adopt a cis-cis conformation with a large affinity for the entering protons, **L2** has been selected for exploring the reactivity of a terdentate fused six-membered chelate with labile metallic cations possessing increasing electrostatic factors along the series $M^{z+} = \text{Li}^+ < \text{Mg}^{2+} \approx \text{Zn}^{2+} < \text{Y}^{3+}$. Spectroscopic, thermodynamic, and structural studies demonstrate that covalency is crucial for stabilizing the complexes $[\text{Zn}(\text{L2})_n]^{2+}$. With the highly charged Y^{3+} cation, hydrolysis drastically competes with ligand complexation, but anhydrous conditions restore sufficient selectivity for the successful coordination of neutral fused six-membered polyaromatic terdentate chelates with large 4f-block cations.



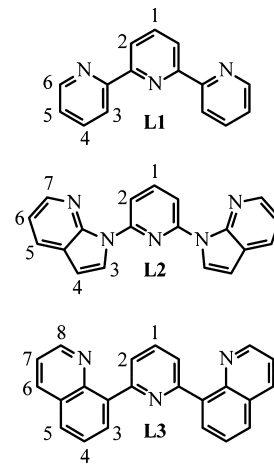
INTRODUCTION

The origin of the systematic preference of large p- and d-block cations for five-membered chelate rings over six-, seven-, or eight-membered analogues has been the subject of intense activity during the late 1980s.¹ Taking cyclopentane and cyclohexane as structural models for these metallocycles, molecular mechanics predicts that only five-membered chelate rings adopt a low strain geometry around a large M^{2+} cation, whereas six-membered rings require too short M-donor bonds ($\sim 1.54 \text{ \AA}$) and too large bite angles ($\sim 109.5^\circ$; Scheme 1).¹ When additional structural constraints are introduced through the incorporation of rigid aromatic units within the chelate ring, the pertinence of this simple analysis becomes debatable, and large trivalent lanthanide cations, Ln^{III} , form stable complexes

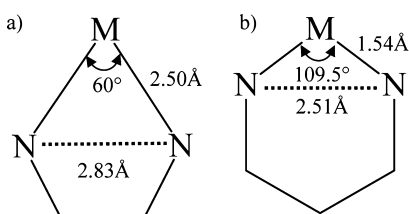
with anionic seven-,² six-,³ and five-membered⁴ aromatic chelate rings (Figure S1 in the Supporting Information, SI).

In this context, neutral N-heterocyclic donor atoms in bidentate 2,2'-bipyridine and terdentate 2,2';6',2"-terpyridine (**L1**; Scheme 2) also provide reasonably stable five-membered chelate complexes with Ln^{III} .^{5,6} Surprisingly, the extended

Scheme 2. Chemical Structures of the Terdentate Ligands L1–L3 with Numbering Schemes for NMR Studies



Scheme 1. Lowest Strain Energy Geometry Calculated Using Molecular Mechanics for (a) a Five-Membered Chelate Ring and (b) a Six-Membered Chelate Ring Adapted from reference 1b

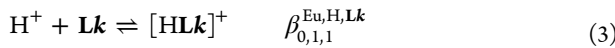
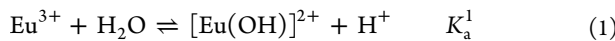


Received: May 29, 2012

Published: July 19, 2012

analogous six-membered chelates 2,6-bis(azaindolyl)pyridine (**L2**)⁷ and 2,6-bis(8-quinolinyl)pyridine (**L3**)⁸ have not been considered for the coordination of Ln^{III} , while some complexes with d-block cations of variable sizes such as Mn^{II} (67 pm),⁹ Cu^{II} (73 pm),¹⁰ Ru^{II} (>82 pm),¹¹ and Pt^{II} (94 pm)¹² have been isolated and characterized in the solid state.

As expected, titration of **L1** with $\text{Eu}(\text{CF}_3\text{SO}_3)_3 \cdot \text{H}_2\text{O}$ in $\text{CD}_3\text{CN}/\text{CDCl}_3$ (1:1) displays the successive formation of $[\text{Eu}(\text{L1})_2\text{S}_3]^{3+}$ and $[\text{Eu}(\text{L1})\text{S}_6]^{3+}$ (S = solvent molecule) characterized by their paramagnetically shifted ^1H NMR signals (Figure S2a in the SI).^{6a} In these complexes, each terpyridine ligand **L1** is meridionally tercoordinated to Ln^{III} , thus producing two fused five-membered chelate rings.⁶ Repeating these titrations with the six-membered chelating ligands **L2** (Figure S2b in the SI) and **L3** (Figure S2c in the SI) shows no trace of paramagnetic effects, but the detection of exchange-broadened spectra on the NMR time scale, which are diagnostic for the formation of the monoprotonated species $[\text{HL2}]^+$ and $[\text{HL3}]^+$ (vide infra). Equilibria (1)–(3) correspond to a simple model rationalizing these observations.



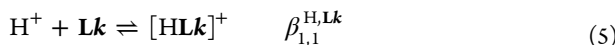
Once K_a^1 is at hand ($K_a^1 = 10^{-8.81}$ in a 0.3 M NaClO_4 aqueous solution),¹³ the competition between ligand complexation (eq 2) and ligand protonation (eq 3) is estimated by the concentration ratio $|[\text{Eu}(\text{Lk})]^{3+}|/|[\text{HLk}]^+|$ given in eq 4 (see Appendix 1 in the SI).

$$\frac{|[\text{Eu}(\text{Lk})]^{3+}|}{|[\text{HLk}]^+|} = \frac{\beta_{1,0,1}^{\text{Eu},\text{H,Lk}}}{\beta_{0,1,1}^{\text{Eu},\text{H,Lk}}} \frac{(|\text{H}_2\text{O}|_{\text{tot}} - |\text{H}_2\text{O}|)}{K_a^1 |\text{H}_2\text{O}|} \quad (4)$$

The exclusive ^1H NMR detection of $[\text{Eu}(\text{L1})]^{3+}$ under stoichiometric conditions ($|[\text{Eu}(\text{Lk})]^{3+}|/|[\text{HLk}]^+| \geq 100$; Figure S2a in the SI) contrasts with the quantitative formation of $[\text{HLk}]^+$ for **L2** and **L3** in the same conditions ($|[\text{Eu}(\text{Lk})]^{3+}|/|[\text{HLk}]^+| \leq 0.01$; Figure S2b,c in the SI). This implies that $\beta_{1,0,1}^{\text{Eu},\text{H,Lk}}/\beta_{0,1,1}^{\text{Eu},\text{H,Lk}}$ drastically decreases for the six-membered chelating ligands **L2** and **L3**, but there is no way to point out the exact influence of each individual contribution (protonation and complexation). Therefore, we first report here on the thermodynamics of the protonation reactions of **L1**–**L3** in $\text{CD}_3\text{CN}/\text{CDCl}_3$, which control the denominator of eq 4. The six-membered chelating ligand with the largest proton affinity ($\beta_{0,1,1}^{\text{M,H,Lk}} = \beta_{1,1}^{\text{H,Lk}}$) is then investigated for its potential complexation properties with labile transition-metal cations, which maximize the numerator of eq 4 (i.e., $\beta_{1,0,1}^{\text{M,H,Lk}}$) in organic solvents.

RESULTS AND DISCUSSION

Protonation of Ligands L1–L3. **L1** is known to bind two successive protons according to equilibria (5) and (6) in water [$\log(\beta_{1,1}^{\text{H,Lk}}) = 4.32(3)$ and $\log(\beta_{1,2}^{\text{H,Lk}}) = 7.59(4)$]¹⁴ and in aqueous organic solvents.¹⁵



^1H NMR titrations of **L1** in $\text{CD}_3\text{CN}/\text{CDCl}_3$ (1:1) with $\text{CF}_3\text{SO}_3\text{H}$ exhibit fast-exchange processes on the NMR time scale (Figure S3 in the SI), and the complete set of weight-average chemical shifts can be satisfactorily fitted to equilibria (5) and (6) by using nonlinear least-squares techniques to give $\log(\beta_{1,1}^{\text{H,Lk}}) = 3.4(1)$ and $\log(\beta_{1,2}^{\text{H,Lk}}) = 5.2(1)$ (Table 1).

Table 1. Cumulative Thermodynamic Protonation Constants [$\log(\beta_{m,1}^{\text{H,Lk}})$], Associated Microscopic Affinities [$\log(f_{\text{connect}}^{\text{H,Lk}})$ and $\Delta G_{\text{connect}}^{\text{H,Lk}}$], Intramolecular Interproton Interactions [$\log(u_{\text{Lk}}^{\text{H,H}})$] and $\Delta G_{\text{interaction}}^{\text{H,H,Lk}}$], and Allosteric Cooperativity Factors (α)^a Obtained by ^1H NMR Titrations of L1–L3 with $\text{CF}_3\text{SO}_3\text{H}$ in $\text{CD}_3\text{CN}/\text{CDCl}_3$ (1:1) at 298 K

	L1	L2	L3
$\log(\beta_{1,1}^{\text{H,Lk}})$	3.4(1)	5.3(3)	2.3(2)
$\log(\beta_{2,1}^{\text{H,Lk}})$	5.2(1)	8.9(3)	5.0(1)
$\log(f_{\text{connect}}^{\text{H,Lk}})$	2.9(1)	4.8(3)	1.8(2)
$\Delta G_{\text{connect}}^{\text{H,Lk}}/(\text{kJ/mol})$	-16.7(6)	-27.5(1.7)	-10.4(1.1)
$\log(u_{\text{Lk}}^{\text{H,H}})$	-1.1(2)	-1.2(5)	0.9(3)
$\Delta G_{\text{interaction}}^{\text{H,H,Lk}}/(\text{kJ/mol})$	6.4(1.0)	7.0(3.0)	-5.0(1.7)
α^a	0.08(3)	0.06(7)	7.5(5.2)

$$^a \alpha = [(\omega_{1,1}^{\text{H,Lk}})^2 / \omega_{2,1}^{\text{H,Lk}}] [\beta_{2,1}^{\text{H,Lk}} / (\beta_{1,1}^{\text{H,Lk}})^2] = 3[\beta_{2,1}^{\text{H,Lk}} / (\beta_{1,1}^{\text{H,Lk}})^2].^{28}$$

Compared with water, the stepwise affinities of **L1** for protons in $\text{CD}_3\text{CN}/\text{CDCl}_3$ are reduced by approximately 1 order of magnitude, which limits the relative quantity of $[\text{HL1}]^+$ and $[\text{H}_2\text{L1}]^{2+}$ formed in solution at millimolar concentrations (Figure 1a).

The individual ^1H NMR spectra computed for **L1**, $[\text{HL1}]^+$, and $[\text{H}_2\text{L1}]^{2+}$ show the systematic downfield shifts of the aromatic protons upon successive protonation (Figure 1b), a trend resulting from a decrease in the electronic density brought on by the protonation of N-heterocyclic aromatic rings in $[\text{HL1}]^+$ and $[\text{H}_2\text{L1}]^{2+}$.¹⁷ Interestingly, the local magnetic environments of the protons H2 and H3 are further sensitive to the cisoid versus transoid conformations adopted by the terdentate ligand (Scheme 3). The abnormal zigzag behavior observed for H3 ($\Delta\delta = 0.45$ ppm on going from **L1** to $[\text{HL1}]^+$ and $\Delta\delta = -0.97$ ppm on going from $[\text{HL1}]^+$ to $[\text{H}_2\text{L1}]^{2+}$; Figure 1b) is diagnostic for the initial protonation of trans-trans terpyridine **L1** (Scheme 3, top)^{18,19} onto one distal pyridine ring to give $[\text{HL1}]^+$, which exists in solution as fast-interconverting cis–trans C_s -symmetrical conformers (Scheme 3, middle),²⁰ followed by the connection of a second proton to give the average coplanar cis–cis isomer in $[\text{H}_2\text{L1}]^{2+}$ (the H3 protons are no more affected by the electronegative nitrogen atoms of the central pyridine ring; Scheme 3, bottom).²¹ This sequence of protonation steps and conformational changes agrees with the molecular structures reported for **L1**,¹⁸ $[\text{HL1}]^+$,²⁰ and $[\text{H}_2\text{L1}]^{2+}$ ²¹ in the solid state (Figure S4 in the SI).

^1H NMR titrations with **L2** (Figure S5 in the SI) and **L3** (Figure S6 in the SI) also show the successive fixation of two protons to give $[\text{HLk}]^+$ (eq 5) and $[\text{H}_2\text{Lk}]^{2+}$ (eq 6, $k = 2, 3$), from which $\log(\beta_{1,1}^{\text{H,Lk}})$ and $\log(\beta_{2,1}^{\text{H,Lk}})$ are obtained by nonlinear least-squares fits (Table 1).¹⁶

Except for a smaller affinity for the connection of the first entering proton, the thermodynamic protonation constants found for **L3** roughly mirror those found for **L1** (Table 1), thus leading to comparable distributions of species in solution (Figures 1a and 2b, top). The stepwise downfield shift of H1 and H6 observed upon protonation of **L3**,¹⁷ combined with the

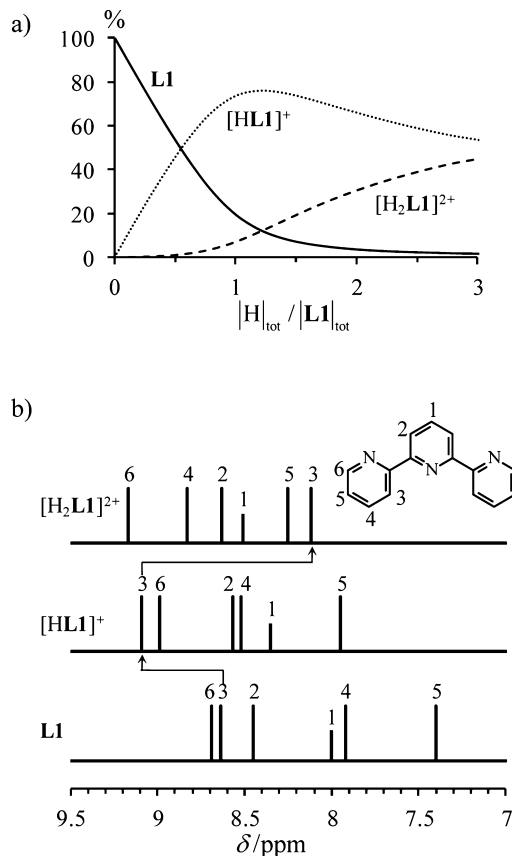
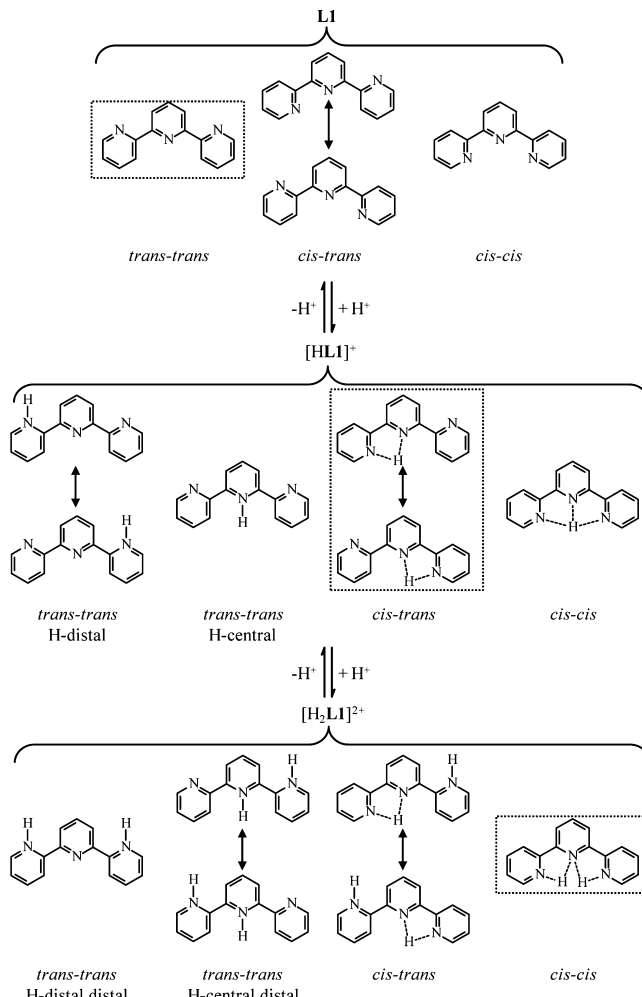


Figure 1. Computed (a) ligand distribution and (b) individual ^1H NMR spectra for L1, $[HL1]^+$, and $[H_2L1]^{2+}$ [$\text{CD}_3\text{CN}/\text{CDCl}_3$ (1:1); total ligand concentration 15 mM; 298 K].

zigzag behavior of H3 (downfield shift $\Delta\delta = 0.95$ ppm on going from L3 to $[HL3]^+$, followed by an upfield shift $\Delta\delta = -0.61$ ppm on going from $[HL3]^+$ to $[H_2L3]^{2+}$; Figure 2b, bottom, and Table S1 in the SI) indicate an average cis-trans conformation for $[HL3]^+$ in solution (as found for $[HL1]^+$), whereas $[H_2L3]^{2+}$ adopts the cis-cis conformation (as found for $[H_2L1]^{2+}$). On the contrary, L2 binds two successive protons with 2 orders of magnitude larger affinities, thus leading to the successive (almost) quantitative formations of $[HL2]^+$ and $[H_2L2]^{2+}$ at stoichiometric ratios for millimolar concentrations (Figure 2a, top). Moreover, the structurally sensitive protons H2 and H3 now exhibit reverse zigzag behaviors (Figure 2a, bottom, and Table S2 in the SI). The initial upfield shifts of H2 and H3 point to the removal of the interaction of these protons with the adjacent nitrogen atoms of the central pyridine ring, as a result of the unusual cis-cis conformation adopted by $[HL2]^+$. The minor additional shift detected upon the addition of a second proton in $[H_2L2]^{2+}$ suggests that the latter conformation is retained in the fully protonated ligand.

In line with the lack of measurable inter-ring H···H nuclear Overhauser enhancement (NOE) effects for the unprotonated ligands in solution, the molecular structures of L1 (Figure S4a, top, in the SI),¹⁸ L2 (Figure 3a, top),¹⁰ and L3 (Figure 4a, top)⁸ in the solid state systematically show the terdentate ligand strand to adopt the trans-trans conformation, which minimizes both steric constraints and intramolecular electric multipolar interactions.^{15,22} Whereas the closest inter-ring interatomic contact distances in L1 [N(distal)···H(central) =

Scheme 3. Possible Dynamically Averaged Conformations Adopted by the Aromatic Tridentate Ligand L1 and Its Protonated Forms $[HL1]^+$ and $[H_2L1]^{2+}$



^aThe conformations observed in the crystal structures and in solution are surrounded.

2.94 Å; Figure S4b, top, in the SI] and in L2 [N(distal)···H(central) = 2.26 Å; Figure 3b, top] are compatible with an approximate coplanar arrangement of the three aromatic rings, L3 displays a significant twist (interplanar pyridine-quinoline angles = 46.4–47.0°; Figure 4b top) for restoring an acceptable contact distance N(distal)···H(central) = 2.65 Å.²³ Protonations of L2 and L3 with $\text{CF}_3\text{SO}_3\text{H}$ in $\text{CH}_2\text{Cl}_2/\text{CH}_3\text{CN}$ (1:1), followed by the slow evaporation or diffusion of diethyl ether yield X-ray-quality prisms for $[HL2](\text{CF}_3\text{SO}_3)$ (1), $[H_2L2]-(\text{CF}_3\text{SO}_3)_2$ (2), $[HL3](\text{CF}_3\text{SO}_3)$ (3), and $[H_2L3](\text{CF}_3\text{SO}_3)_2$ (4). Each structure is constituted of protonated cations displaying weak (if any) contacts with ionic triflate counter-anions (Tables S2–S14 and Figures S7–S10 in the SI).^{24,25} Similarly to $[HL1]^+$, the molecular structure of the monoprotonated six-membered analogue $[HL3]^+$ adopts a pseudo-cis-trans conformation, in which the two rings interacting with the entering proton are coplanar (interplanar pyridine-quinoline angle = 3.4°; Table S10 in the SI and Figure 4, middle). The additional hydrogen atom is located on the nitrogen atom of the central pyridine ring, and it forms a bent hydrogen bond with the nitrogen atom of the adjacent coplanar quinoline ring (Figure 4b, middle, and Figure S8a and

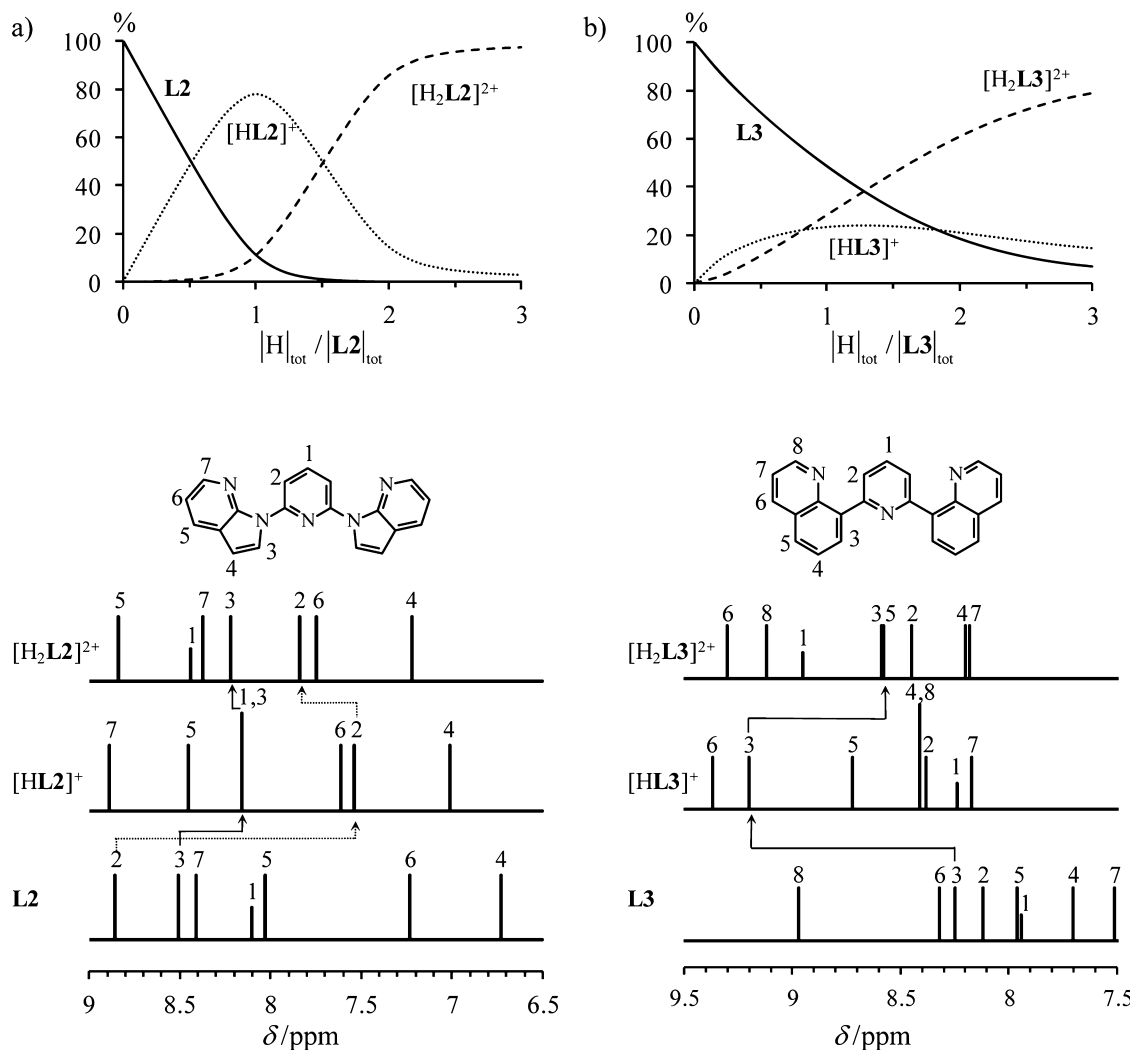


Figure 2. Computed ligand distribution and individual ^1H NMR spectra for (a) $\text{L}2$, $[\text{HL}2]^+$, and $[\text{H}_2\text{L}2]^{2+}$ and (b) $\text{L}3$, $[\text{HL}3]^+$, and $[\text{H}_2\text{L}3]^{2+}$ ($\text{CD}_3\text{CN}/\text{CDCl}_3$ (1:1); total ligand concentration 15 mM; 298 K].

Table S11 in the SI). In excess of acid, the two distal quinoline rings are protonated in $[\text{H}_2\text{L}3]^{2+}$, which adopts the *cis–cis* conformation similarly observed for $[\text{H}_2\text{L}1]^{2+}$, but twisted along the aromatic backbone (interplanar pyridine–quinoline angles = 23.9–31.6°; Table S13 in the SI and Figure 4, bottom). Two weak and bent intramolecular hydrogen bonds contribute to stabilization of the molecular edifice (Figure 4, bottom, and Table S14 and Figure S8b in the SI). The situation is quite different for $[\text{HL}2]^+$, because the entering proton is trapped within a cavity of three nitrogen atoms brought by the coplanar *cis–cis* arrangement of the three aromatic rings (interplanar pyridine–azaindole angles = 3.7–4.2°; Table S4 in the SI and Figure 3, middle). A bifurcated hydrogen bond links the distal N(azaindole)–H donor with the two adjacent nitrogen atoms of the other aromatic rings (Table S5 and Figure S7a in the SI). The fixation of the second proton in $[\text{H}_2\text{L}2]^{2+}$ occurs on the second azaindole ring, which produces the usual helical twist of the polyaromatic backbone (interplanar azaindole–pyridine rings = 20.9–31.7°; Table S7 in the SI and Figure 3, bottom) stabilized by weak bent hydrogen bonds (Figure 3, bottom, and Table S8 and Figure S7 in the SI).

We conclude that the solution structures established by ^1H NMR fairly agree with the molecular structures observed in the

solid state. For $\text{L}1$ and $\text{L}3$, the thermodynamic protonation constants are comparable and the *trans–trans-Lk* arrangement found for the nonprotonated ligands transforms into *cis–trans*– $[\text{HL}k]^+$ and *cis–cis*– $[\text{H}_2\text{L}k]^{2+}$. For $\text{L}2$, the protonation steps are thermodynamically more favorable because the initial coplanar *trans–trans-L2* arrangement is transformed into coplanar *cis–cis* conformations in both $[\text{HL}2]^+$ and $[\text{H}_2\text{L}2]^{2+}$.

Taking the molecular structures of *cis–cis*– $[\text{H}_2\text{L}k]^{2+}$ ($k = 1–3$) as rough models for the meridional teroordination of these ligands around multivalent cations, the fused polyaromatic five-membered chelate rings in $\text{L}1$ mainly differ from the fused polyaromatic six-membered chelate rings in $\text{L}2$ and $\text{L}3$ by the geometry of the pseudoisosceles triangles drawn by the three nitrogen donor atoms (Figure 5). For each triangle, the nitrogen atom of the central pyridine ring occupies the apex position, but only $[\text{H}_2\text{L}1]^{2+}$ possesses an obtuse apex angle, which leads to a flattened arrangement of the three nitrogen donor atoms compatible with the encapsulation of large cations ($d_{\text{N}(\text{distal})–\text{N}(\text{distal})} = 4.55 \text{ \AA}$; Figure 5a). The acute isosceles triangles observed for $[\text{H}_2\text{L}2]^{2+}$ and $[\text{H}_2\text{L}3]^{2+}$ result in shorter $\text{N}(\text{distal})\cdots\text{N}(\text{distal})$ contact distances (3.39–3.64 Å; Figure 5b,c), which are expected to be less favorable for the approach of large cations.

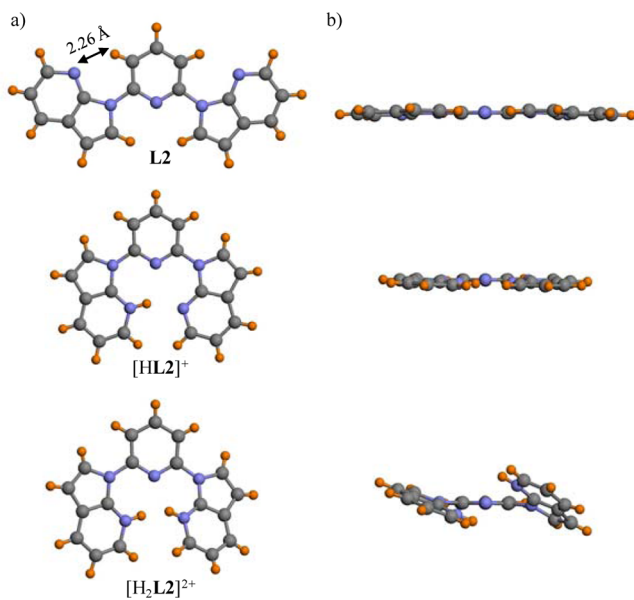


Figure 3. Perspective views (a) perpendicular and (b) parallel to the central pyridine ring of the molecular structures of L2, $[HL2]^+$, and $[H_2L2]^{2+}$ observed in the crystal structures of L2,¹⁰ 1, and 2. Color code: gray, C; blue, N; orange, H.

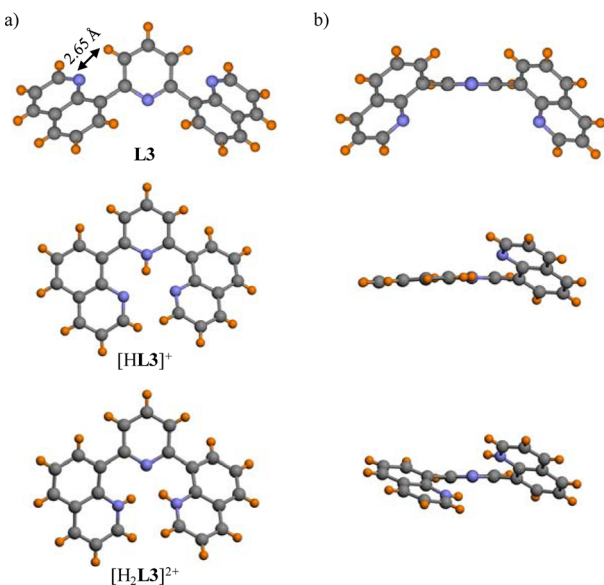


Figure 4. Perspective views (a) perpendicular and (b) parallel to the central pyridine ring of the molecular structures of L3, $[HL3]^+$, and $[H_2L3]^{2+}$ observed in the crystal structures of L3,⁸ 3, and 4. Color code: gray, C; blue, N; orange, H.

Thermodynamic Modeling for the Protonation Steps in Ligands L1–L3. Within the frame of the site-binding approach,²⁶ the cumulative protonation constants (eqs 5 and 6) can be modeled with eqs 7 and 8, respectively.

$$\beta_{1,1}^{H,Lk} = \omega_{1,1}^{H,Lk}(\text{distal}) f_{\text{distal}}^{H,Lk} + \omega_{1,1}^{H,Lk}(\text{central}) f_{\text{central}}^{H,Lk} \quad (7)$$

$$\beta_{2,1}^{H,Lk} = \omega_{1,1}^{H,Lk}(\text{distal}) (f_{\text{distal}}^{H,Lk})^2 u_{d,d,Lk}^{H,H} + \omega_{2,1}^{H,Lk}(\text{central}) (f_{\text{central}}^{H,Lk}) (f_{\text{distal}}^{H,Lk}) u_{c,d,Lk}^{H,H} \quad (8)$$

In these equations, $\omega_{n,1}^{H,Lk}$ takes into account the pure statistical (i.e., entropic) contribution due to a change in the molecular

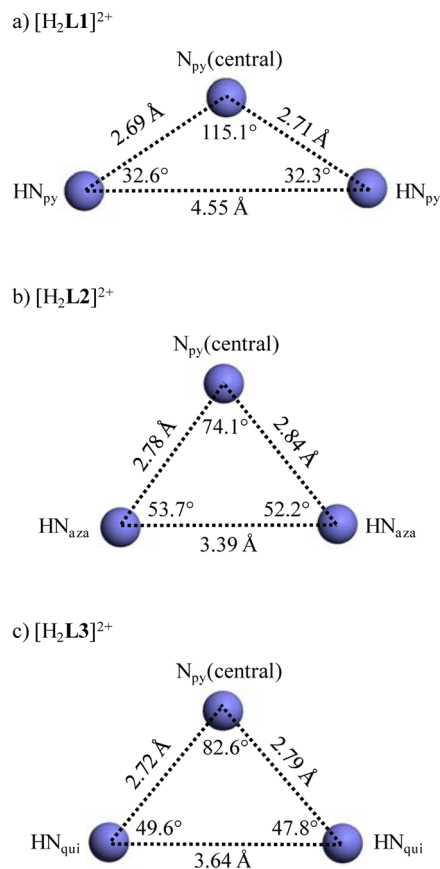


Figure 5. Geometries of the pseudoisosceles triangles formed by the nitrogen donor atoms in the molecular structures of (a) $[H_2L1]^{2+}$, (b) $[H_2L2]^{2+}$ and (c) $[H_2L3]^{2+}$.

rotational entropies occurring upon protonation.²⁷ Once the point group of each partner contributing to equilibria (5) and (6) is at hand, $\omega_{n,1}^{H,Lk}$ values are easily computed using the method of symmetry numbers (Figures S14 and S15 in the SI).²⁷ $f_{\text{distal}}^{H,Lk}$ and $f_{\text{central}}^{H,Lk}$ correspond to the absolute affinities of the distal and central heterocyclic aromatic rings, respectively, for its intermolecular connection with a proton. Application of the van't Hoff isotherm transforms these thermodynamic descriptors into free energies of connection $\Delta G_{\text{distal}}^{H,Lk} = -RT \ln(f_{\text{distal}}^{H,Lk})$ and $\Delta G_{\text{central}}^{H,Lk} = -RT \ln(f_{\text{central}}^{H,Lk})$, which include desolvation processes (the standard concentration of the reference state is set to 1 M).^{26d} Finally, $u_{d,d,Lk}^{H,H} = \exp[-(\Delta E_{d,d,Lk}^{H,H}/RT)]$ and $u_{c,d,Lk}^{H,H} = \exp[-(\Delta E_{c,d,Lk}^{H,H}/RT)]$ are the Boltzmann factors correcting the free energy of connection for any intramolecular H···H interactions resulting from the close location of the two protons in $[H_2Lk]^{2+}$ (d,d = distal-distal interactions and c,d = central-distal interactions). Taking into account the structural information brought by the combination of ¹H NMR and X-ray crystal structures, two averaged coplanar trans-cis conformers contribute to the macrospecies $[HLk]^+$ in solution (i.e., protonation occurring either on the central or on the distal cis-aromatic rings; Figure S14 in the SI) and two averaged coplanar cis-cis conformers contribute to the macrospecies $[H_2Lk]^{2+}$ (i.e., protonations occurring either on the central-distal or on the distal-distal pair positions of the aromatic rings; Figure S15 in the SI). Consequently, each associated macroconstant in eqs 7 and 8 combines two microconstants, eventually leading to eqs 10 and 11 after the introduction of adequate statistical factors.

$$\beta_{1,1}^{H,Lk} = 2f_{\text{distal}}^{H,Lk} + f_{\text{central}}^{H,Lk} \quad (10)$$

$$\begin{aligned} \beta_{2,1}^{H,Lk} &= \omega_{1,1}^{H,Lk}(\text{distal}) (f_{\text{distal}}^{H,Lk})^2 u_{d,d,Lk}^{H,H} + \omega_{2,1}^{H,Lk}(\text{central}) \\ &\quad (f_{\text{central}}^{H,Lk}) (f_{\text{distal}}^{H,Lk}) u_{c,d,Lk}^{H,H} \end{aligned} \quad (11)$$

Reasonably assuming for each specific ligand **Lk** that (i) the affinity of the proton for the central and distal aromatic rings are comparable ($f_{\text{distal}}^{H,Lk} \approx f_{\text{central}}^{H,Lk} = f_{\text{connect}}^{H,Lk}$) and (ii) the interproton interactions operating within each microspecies contributing to $[\text{H}_2\text{Lk}]^{2+}$ are similar $u_{d,d,Lk}^{H,H} \approx u_{c,d,Lk}^{H,H} = u_{\text{Lk}}^{H,H}$, eqs 10 and 11 reduce to

$$\beta_{1,1}^{H,Lk} = 3f_{\text{connect}}^{H,Lk} \quad (12)$$

$$\beta_{2,1}^{H,Lk} = 3(f_{\text{connect}}^{H,Lk})^2 u_{\text{Lk}}^{H,H} \quad (13)$$

Introducing the experimental protonation constants $\beta_{1,1}^{H,Lk}$ and $\beta_{2,1}^{H,Lk}$ collected for each ligand (Table 1, entries 1 and 2) into eqs 12 and 13 provides $\log(f_{\text{connect}}^{H,Lk})$ (Table 1, entry 3) and $\log(u_{\text{Lk}}^{H,H})$ (Table 1, entry 5), from which the associated free energy changes $\Delta G_{\text{connect}}^{H,Lk} = -RT \ln(f_{\text{connect}}^{H,Lk})$ (Table 1, entry 4) and $\Delta E_{\text{interaction}}^{H,H,Lk} = -RT \ln(u_{\text{Lk}}^{H,H})$ (Table 1, entry 6) are deduced. We immediately notice that $\Delta G_{\text{connect}}^{H,L2} \ll \Delta G_{\text{connect}}^{H,L1} \leq \Delta G_{\text{connect}}^{H,L3}$, a trend resulting from the special ability of $[\text{H}_n\text{L2}]^{n+}$ for adopting the cis-cis conformation, in which the three adjacent nitrogen donor atoms contribute to the fixation of the entering protons. In line with straightforward electrostatic arguments, the fixation of a second proton to $[\text{HLk}]^+$ to give $[\text{H}_2\text{Lk}]^{2+}$ ($k = 1, 2$) is anticooperative ($\Delta E_{\text{interaction}}^{H,H,L1} \approx \Delta E_{\text{interaction}}^{H,H,L2} \approx 7 \text{ kJ/mol}$; allosteric cooperativity factor $\alpha < 1$; Table 1, entry 7).²⁸ Surprisingly, the reverse situation is found for **L3**, for which complexation of the second proton is driven to completion by a slightly positive cooperative process [$\Delta E_{\text{interaction}}^{H,H,L3} = -5.0(1.7) \text{ kJ/mol}$; allosteric cooperativity factor $\alpha > 1$; Table 1, entry 7]. Let us now rearrange the general form of the competition equilibrium (4) for **L2** and **L3**.

$$\begin{aligned} \frac{|\text{[Eu(Lk)}^{3+}]|}{|\text{[HLk}^+]|} &= \frac{\beta_{1,0,1}^{\text{Eu},\text{H,Lk}}}{\beta_{0,1,1}^{\text{Eu},\text{H,Lk}}} \frac{(|\text{H}_2\text{O}|_{\text{tot}} - |\text{H}_2\text{O}|)}{K_a^1 |\text{H}_2\text{O}|} \\ &\leq 0.01 \Rightarrow \beta_{1,0,1}^{\text{Eu},\text{H,Lk}} \leq \frac{0.01 K_a^1 - |\text{H}_2\text{O}|}{(|\text{H}_2\text{O}|_{\text{tot}} - |\text{H}_2\text{O}|)} \beta_{0,1,1}^{\text{Eu},\text{H,Lk}} \end{aligned} \quad (14)$$

Because $\beta_{0,1,1}^{\text{Eu},\text{H,L2}} = \beta_{1,1}^{\text{H,L2}}$ is 3 orders of magnitude larger than $\beta_{1,1}^{\text{H,L3}}$ under the same experimental conditions, we deduce that **L2** is a much better candidate than **L3** for the formation of stable six-membered complexes with large labile cations.

Complexation of Ligand **L2** with Li^I, Mg^{II}, Zn^{II}, and Y^{III}.

Electrospray ionization mass spectrometry (ESI-MS) titrations of **L2** with LiClO₄ or Mg(ClO₄)₂ ($|\text{L2}|_{\text{tot}} = 0.5 \text{ mM}$ in CH₃CN/CHCl₃ (1:1); $|\text{M}|_{\text{tot}}/|\text{L2}|_{\text{tot}} = 0.1-100$) mainly show the signal of the protonated ligand $[\text{HL2}]^+$ (m/z 311.5), together with weak peaks corresponding to $[\text{Li}(\text{L2})]^+$ (m/z 318.5), $[\text{Li}_2(\text{L2})-(\text{CH}_3\text{CN})_2]^{2+}$ (m/z 204.9), $[\text{Mg}(\text{L2})_2]^{2+}$ (m/z 323.5), and $[\text{Mg}(\text{L2})(\text{ClO}_4)]^+$ (m/z 434.0). Parallel ¹H NMR titrations performed in the same solvent mixture with $|\text{L2}|_{\text{tot}} = 7.5 \text{ mM}$ show faint evolution of the spectra for Li^I, where only a massive excess of Li^I produces some noticeable changes (Figure S16 in the SI). The larger electrostatic factor $z^2/R = 5.56 \text{ eu}/\text{\AA}$ calculated for Mg²⁺ improves the interaction with the nitrogen donor atoms of **L2**,²⁹ and ¹H NMR titrations in the range $|\text{Mg}|_{\text{tot}}/|\text{L2}|_{\text{tot}} = 0.1-1.0$ evidence upfield shifts for H2 and H3,

which are diagnostic for the meridional tercoordination of the ligand around Mg^{II} (Figure S17 in the SI). The unfavorable intermediate dynamic exchange regime operating on the NMR time scale at 298 K with Mg^{II} prevents a quantitative analysis of the thermodynamic complexation process in these conditions. With Zn^{II}, the lower energy of the empty metal-centered 4s orbitals favors covalent interactions with soft nitrogen donor ligands⁶ⁱ and ¹H NMR titrations of **L2** with Zn(CF₃SO₃)₂ show the successive formation of $[\text{Zn}(\text{L2})_2]^{2+}$ and $[\text{Zn}(\text{L2})]^{2+}$, which are in slow exchange on the NMR time scale (Figure S18 in the SI). The thorough integration of the signals of the various protons belonging to the three species **L2**, $[\text{Zn}(\text{L2})_2]^{2+}$, and $[\text{Zn}(\text{L2})]^{2+}$ along the titration process provides fair estimations for the thermodynamic stability constants associated with eqs 15 and 16 (Figure 6a and Appendix 2 in the SI).

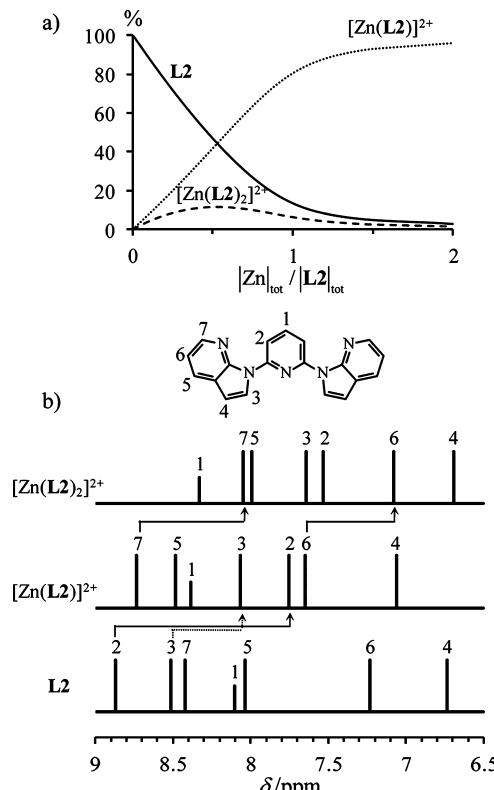
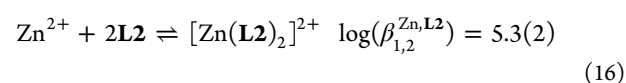
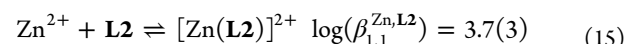


Figure 6. Computed (a) ligand distribution and (b) individual ¹H NMR spectra for **L2**, $[\text{Zn}(\text{L2})]^{2+}$, and $[\text{Zn}(\text{L2})_2]^{2+}$ [CD₃CN/CDCl₃ (1:1); total ligand concentration 7.5 mm; 298 K].

The upfield shifts of H2 and H3 point to the usual meridional tercoordination (i.e., cis-cis conformation) of **L2** to Zn^{II} in the two complexes (Figure 6b and Table S1 in the SI) as substantiated by the molecular structure of $[\text{Zn}(\text{L2})-(\text{CF}_3\text{SO}_3)_2]$ (**6**) deduced from X-ray diffraction studies (Figure 7 and Tables S18-S20 in the SI). The asymmetric unit in **6** contains two independent slightly different molecules A and B related by $\pi-\pi$ -stacking interactions (Figure S19 in the SI). Because B- $[\text{Zn}(\text{L2})_2](\text{CF}_3\text{SO}_3)_2$ is less disordered, it will be

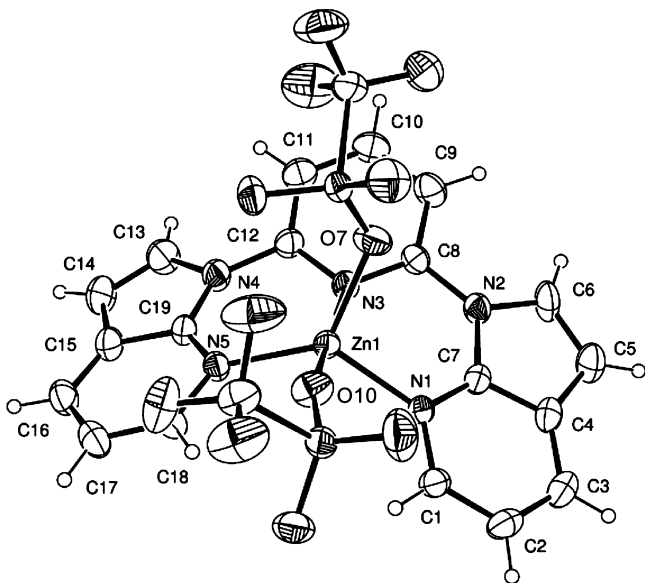


Figure 7. ORTEP view of **6** (complex B) observed in the crystal structure of **6** with an atomic numbering scheme. Thermal ellipsoids are represented at the 50% probability level.

considered for the discussion of the molecular structure (Figure 7).

In order to accommodate acceptable Zn–N bond distances in the 1.98–2.25 Å range (Table S19 in the SI), the bound ligand **L2** is severely twisted (intramolecular azaindole–pyridine interplanar angles = 25–28°; Table S20 in the SI), as was previously noticed for $[\text{Cu}(\text{L2})(\text{NO}_3)_2]$ (interplanar angle = 23.0°).¹⁰ However, the overall helical twist found in the latter complex or in analogous palladium(II) and platinum(II) complexes^{12,30,31} is replaced with a butterfly conformation in $[\text{Zn}(\text{L2})](\text{CF}_3\text{SO}_3)_2$ (**6**; Figure S20 in the SI). This produces

an unprecedented axially elongated pseudobipyramidal-trigonal arrangement of the five donor atoms about Zn^{II}, with N3 and O10 occupying the axial position and N1, N5, and O7 forming the trigonal basis (Figure 7). The nonplanarity of the polyaromatic backbone is characteristic for the tercoordination of the fused six-membered chelate rings **L2**^{10,12} and **L3**^{9,11} to the metal, which contrasts with the planar arrangement of the terpyridine ligand in $[\text{Zn}(\text{L1})\text{Br}_2]$ (twist angle < 1°).³¹ The associated loss in aromaticity explains the low stability constants $\log(\beta_{1,1}^{\text{Zn},\text{L2}}) = 3.7(3)$ (eq 15) observed for $[\text{Zn}(\text{L2})]^{2+}$, which is 4 orders of magnitude weaker than that reported for $[\text{Zn}(\text{L1})]^{2+}$ (water, ionic strength = 0).⁶ⁱ The fixation of a second ligand to give $[\text{Zn}(\text{L2})_2]^{2+}$ is almost statistical (vide infra), and the latter complex counts for less than 10% of the ligand speciation at millimolar concentrations (Figure 6a). We, however, note the considerable upfield shifts of the ¹H NMR signals of the terminal protons H6 and H7 on going from $[\text{Zn}(\text{L2})]^{2+}$ to $[\text{Zn}(\text{L2})_2]^{2+}$, a behavior diagnostic for their location in the shielding region of the second aromatic ligand bound to the same metal in pseudooctahedral bis-terdentate complexes.³² Applying the thermodynamic site-binding model to eqs 15 and 16 gives eqs 17 and 18, from which the free energy of connection of Zn^{II} to the tridentate binding ligand **L2** [$\Delta G_{\text{connect}}^{\text{Zn},\text{L2}} = -RT \ln(G_{\text{connect}}^{\text{Zn},\text{L2}}) = -11.5(1.7)$ kJ/mol] can be estimated, together with a negligible anticooperative interligand interaction [$\Delta E_{\text{Zn}}^{\text{L2},\text{L2}} = -RT \ln(u_{\text{Zn}}^{\text{L2},\text{L2}}) = 0.7(2.7)$ kJ/mol; Figure S21 in the SI].

$$\beta_{1,1}^{\text{Zn},\text{L2}} = 48f_{\text{connect}}^{\text{Zn},\text{L2}} \quad (17)$$

$$\beta_{2,1}^{\text{Zn},\text{L2}} = 24(f_{\text{connect}}^{\text{Zn},\text{L2}})^2 u_{\text{Zn}}^{\text{L2},\text{L2}} \quad (18)$$

Because $\Delta G_{\text{connect}}^{\text{Zn},\text{L2}} \gg \Delta G_{\text{connect}}^{\text{H,L2}}$, competition with protonation is expected to be very severe, in line with the quantitative formation of $[\text{HL2}]^+$ upon the reaction of **L2** with triply charged Eu³⁺ in a wet solvent (Figure S2b in the SI). With

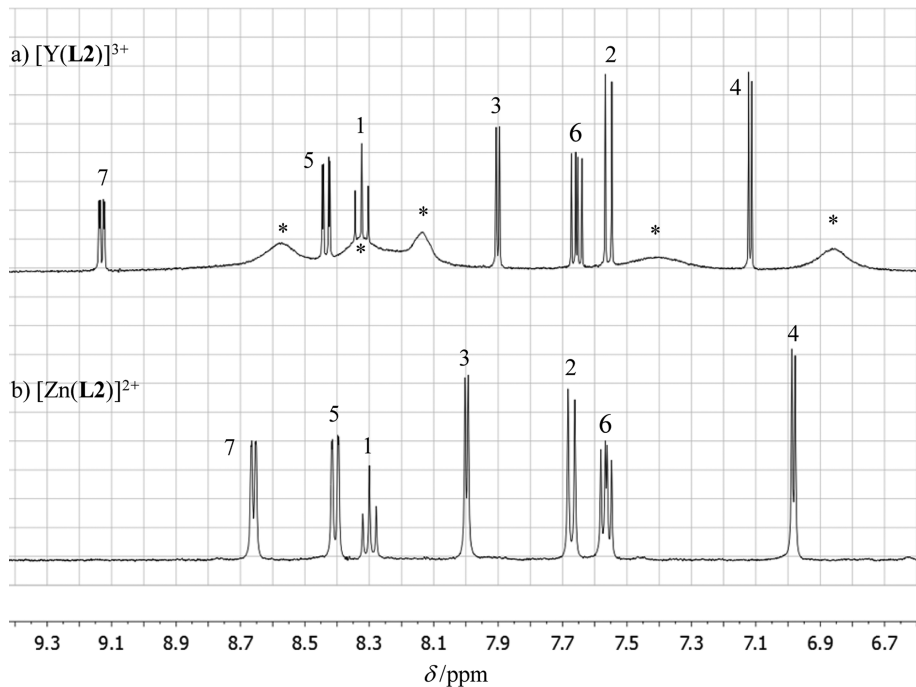


Figure 8. ¹H NMR spectra of (a) $[\text{Y}(\text{L2})]^{3+}$ (CD_2Cl_2) and (b) $[\text{Zn}(\text{L2})]^{2+}$ [$\text{CD}_2\text{Cl}_2/\text{CD}_3\text{CN}$ (1:1)] at 298 K. Asterisks indicate residual signals of $[\text{Y}(\text{L2})_2]^{3+}$.

these thermodynamic results in mind, we decided to react **L2** (7.5 mM) with anhydrous YI_3 in dry CD_2Cl_2 in order to remove traces of competing protons. Because of the minor solubility of YI_3 in this solvent, we are limited to $[\text{YI}_3]_{\text{tot}}/[\text{L2}]_{\text{tot}} < 1.0$, but we undeniably observe the formation of $[\text{Y}(\text{L2})]^{3+}$ as the major component in the mixture, together with the residual dynamically broadened upfield-shifted signals of $[\text{Y}(\text{L2})_2]^{3+}$ (Figure 8a and Table S1 in the SI). The ^1H NMR spectrum recorded for $[\text{Y}(\text{L2})]^{3+}$ closely matches that obtained for $[\text{Zn}(\text{L2})]^{2+}$ (Figure 8b) and points to very similar conformations for the bound tridentate ligand around the metals. The noticeable 0.35 ppm downfield shift of H_7 in $[\text{Y}(\text{L2})]^{3+}$ confirms the larger positive charge born by Y^{III} .¹⁷

CONCLUSION

The insertion of an additional phenyl ring between the distal and central pyridine rings on going from **L1** (five-membered chelate ligand) to **L3** (six-membered chelate ligand) has only minor effects on the global thermodynamic of protonation in $\text{CD}_3\text{CN}/\text{CDCl}_3$, with both systems requiring a large excess of acids for their quantitative diprotonation at millimolar concentrations. The reluctance of **L3** for binding large lanthanide cations can be thus safely assigned to the weak affinity of this latter ligand for Eu^{III} ($\beta_{1,0,1}^{\text{Eu},\text{H},\text{L}3} \ll \beta_{1,0,1}^{\text{Eu},\text{H},\text{L}1}$). According to a geometrical point of view, the transformation of the obtuse isosceles triangle drawn by the three nitrogen donor atoms in the cis–cis conformation of $[\text{H}_2\text{L1}]^{2+}$ into an acute isosceles triangle in $[\text{H}_2\text{L3}]^{2+}$ supports the difficult incorporation of large cations by two fused six-membered chelate rings. The considerable affinity of **L2** for the entering proton contrasts with this picture ($\beta_{1,1}^{\text{H},\text{L}2} \gg \beta_{1,1}^{\text{H},\text{L}1}, \beta_{1,1}^{\text{H},\text{L}3}$), and **L2** indeed complexes larger labile cations Mg^{II} , Zn^{II} , and Y^{III} at millimolar concentrations. Although modest, the formation constants estimated for $[\text{Zn}(\text{L2})_n]^{2+}$ are compatible with exploration of the selectivity induced by this novel class of neutral N-heterocyclic ligands along the 3d- and 4f-block series.

EXPERIMENTAL SECTION

Chemicals were purchased from Strem, Acros, Fluka AG, and Aldrich and used without further purification unless otherwise stated. The trifluoromethanesulfonate salt $\text{Eu}(\text{CF}_3\text{SO}_3)_3 \cdot \text{H}_2\text{O}$ was prepared from the corresponding oxide (Aldrich, 99.99%).³³ $\text{YI}_3(\text{THF})_{3,5}$ was isolated from the reaction of elemental iodine with powdered yttrium metal.³⁴ The ligands **L2**⁷ and **L3**⁸ were prepared according to literature procedures. We were, however, unable to reproduce the 80% yield reported for the Suzuki–Miyaura cross-coupling leading to **L3** (Appendix 3). Silica gel plates Merck 60F₂₅₄ were used for thin layer chromatography, and Fluka silica gel 60 (0.04–0.063 mm) or Acros neutral activated alumina (0.050–0.200 mm) was used for preparative column chromatography.

Preparation of $[\text{Zn}(\text{L2})](\text{CF}_3\text{SO}_3)_2$ (6). Stoichiometric amounts of **L2** (50 mg, 0.16 mmol) and $\text{Zn}(\text{CF}_3\text{SO}_3)_2$ (59.3 mg, 0.16 mmol) were reacted in acetonitrile/dichloromethane (1:1; 10 mL) at room temperature for 2 h. The solvent was evaporated, and the resulting white-off solid was dissolved in acetonitrile (3 mL). The slow diffusion of diethyl ether afforded X-ray-quality prisms of **6** (63.4 mg, 92.5 μmol , 56% yield). ^1H NMR [$\text{CDCl}_3/\text{CD}_3\text{CN}$ (1:1), 400 MHz]: δ 8.74 (dd, 2H, $^3J = 5.4$ MHz, $^4J = 1.4$ MHz), 8.49 (dd, 2H, $^3J = 7.9$ MHz, $^4J = 1.5$ MHz), 8.39 (t, 1H, $^3J = 5.4$ MHz), 8.08 (d, 2H, $^3J = 4$ MHz), 7.76 (d, 2H, $^3J = 8.3$ MHz), 7.66 (dd, 2H, $^3J = 7.8$ MHz, $^4J = 5.4$ MHz), 7.07 (d, 2H, $^3J = 4$ MHz). Elem anal. Calcd for $\text{ZnC}_{21}\text{H}_{13}\text{N}_5\text{O}_6\text{S}_2\text{F}_6$: C, 37.37; H, 1.94; N, 10.38. Found: C, 37.27; H, 2.05; N, 10.19.

Spectroscopic Measurements. ^1H and ^{13}C NMR spectra were recorded on a Bruker Avance 400 MHz spectrometer. Chemical shifts

are given in ppm with respect to tetramethylsilane. In a typical ^1H NMR titration experiment, 500 μL of a 7.5×10^{-3} M solution of ligand **Lk** in $\text{CD}_3\text{CN}/\text{CDCl}_3$ (1:1) were reacted with successive aliquots of solutions of $\text{CF}_3\text{SO}_3\text{H}$, LiClO_4 , $\text{Mg}(\text{ClO}_4)_2$, $\text{Zn}(\text{CF}_3\text{SO}_3)_2$, or $\text{YI}_3(\text{THF})_{3,5}$ in the same solvent mixture. After each aliquot, the ^1H NMR spectrum was recorded at 298 K and the global chemical shift matrix was fitted to equilibria (5) and (6) by using HypNMR-2008 software.¹⁶ Pneumatically assisted electrospray (ESI-MS) mass spectra were recorded from 10^{-4} M solutions on an Applied Biosystems API 150EX LC/MS system equipped with a Turbo Ionspray source. Elemental analyses were performed by K. L. Buchwalder from the Microchemical Laboratory of the University of Geneva.

X-ray Crystallography. The crystal data, intensity measurements, and structure refinements for **1–4**, $[\text{H}_2\text{L2}]_{\text{I}2}$ (5), and 6 were collected in Tables S2 and S18 (SI). All crystals were mounted on quartz fibers with protection oil. Cell dimensions and intensities were measured at 180 or 293 K on a Agilent Supernova diffractometer with mirror-monochromated Cu-K α radiation ($\lambda = 1.54184$ Å). Data were corrected for Lorentz and polarization effects and for absorption. The structures were solved by direct methods (*SIR97*);³⁵ all other calculations were performed with *SHELX97*³⁶ systems and *ORTEP3*³⁷ programs. CCDC 853589–853592 (1–4) and CCDC 883807 and 883808 (5 and 6) contain the supplementary crystallographic data. The CIF files can be obtained free of charge via www.ccdc.cam.ac.uk/conts/retrieving.html (or from the Cambridge Crystallographic Data Centre, 12 Union Road, Cambridge CB2 1EZ, U.K.; fax (+44) 1223-336-033 or deposit@ccdc.cam.ac.uk).

ASSOCIATED CONTENT

S Supporting Information

Derivation of eq 4 (Appendix 1), speciation for the zinc(II) complexes (Appendix 2), and experimental synthetic parts for **L2**, **L3**, and $\text{YI}_3(\text{THF})_{3,5}$ (Appendix 3), tables of ^1H NMR chemical shifts, data crystal data, geometric parameters, bond distances, and bond angles, figures showing molecular structures with numbering schemes and crystal packing, symmetry numbers, and ^1H NMR titrations, and a CIF file for compounds **1–6**. This material is available free of charge via the Internet at <http://pubs.acs.org>.

AUTHOR INFORMATION

Corresponding Author

*E-mail: Claude.Piguet@unige.ch.

Notes

The authors declare no competing financial interest.

ACKNOWLEDGMENTS

Financial support from the Swiss National Science Foundation is gratefully acknowledged.

REFERENCES

- (a) Hancock, R. D. *J. Chem. Educ.* **1992**, *69*, 615–621. (b) Motekaitis, R. J.; Martell, A. E.; Hancock, R. D. *Coord. Chem. Rev.* **1994**, *133*, 39–65 and references cited therein.
- (a) Gan, X.-M.; Duesler, E. N.; Paine, R. T. *Inorg. Chem.* **2001**, *40*, 4420–4427. (b) Paine, R. T.; Tan, Y.-C.; Gan, X.-M. *Inorg. Chem.* **2001**, *40*, 7009–7013. (c) Huskowska, E.; Turowska-Tyrk, I.; Legendziewicz, J.; Riehl, J. P. *New J. Chem.* **2002**, *26*, 1461–1467. (d) Gan, X.; Rapko, B. M.; Duesler, E. N.; Binyamin, I.; Paine, R. T.; Hay, B. P. *Polyhedron* **2005**, *24*, 469–474. (e) Binyamin, I.; Pailloux, S.; Duesler, E. N.; Rapko, B. M.; Paine, R. T. *Inorg. Chem.* **2006**, *45*, 5886–5892. (f) Pailloux, S.; Shirima, C. E.; Ray, A. D.; Duesler, E. N.; Paine, R. T.; Klaehn, J. R.; McIlwain, M. E.; Hay, B. P. *Inorg. Chem.* **2009**, *48*, 3104–3113. (g) Eliseeva, S. V.; Pleshkov, D. N.; Lyssenko, K. A.; Lepnev, L. S.; Bünzli, J.-C. G.; Kuzmina, N. P. *Inorg. Chem.* **2011**, *50*, 5137–5144.

- (3) (a) Laus, S.; Ruloff, R.; Toth, E.; Merbach, A. E. *Chem.—Eur. J.* **2003**, *9*, 3555–3566. (b) Polasek, M.; Rudovsky, J.; Hermann, P.; Lukes, I.; Vander Elst, L.; Muller, K. N. *Chem. Commun.* **2004**, 2602–2603. (c) Moore, E. G.; Samuel, A. P. S.; Raymond, K. N. *Acc. Chem. Res.* **2009**, *42*, 542–552 and references cited therein.
- (4) (a) Wu, S. L.; Horrocks, W. deW. *J. Chem. Soc., Dalton Trans.* **1997**, 1497–1502. (b) Elhabiri, M.; Scopelliti, R.; Bünzli, J.-C. G.; Piguet, C. *J. Am. Chem. Soc.* **1999**, *121*, 10747–10762. (c) Datta, A.; Raymond, K. N. *Acc. Chem. Res.* **2009**, *42*, 938–947 and references cited therein. (d) Tei, L.; Baranyai, Z.; Brücher, E.; Cassino, C.; Demicheli, F.; Masciocchi, N.; Giovenzana, G. B.; Botta, M. *Inorg. Chem.* **2010**, *49*, 616–625.
- (5) (a) Semenova, L. J.; Skelton, B. W.; White, A. H. *Aust. J. Chem.* **1999**, *52*, 551–569. (b) Semenova, L. J.; White, A. H. *Aust. J. Chem.* **1999**, *52*, 571–600. (c) van Staveren, D. R.; van Albada, G. A.; Haasnoot, J. G.; Kooijman, H.; Lanfredi, A. M. M.; Neuwenhuizen, P. J.; Spek, A. L.; Ugozzoli, F.; Weyermüller, T.; Reedijk, J. *Inorg. Chim. Acta* **2001**, *315*, 163–171. (d) Puntus, L. N.; Lyssenko, K. A.; Pekareva, I. S.; Bünzli, J.-C. G. *J. Phys. Chem. B* **2009**, *113*, 9265–9277. (e) Kubicek, V.; Hamplova, A.; Maribé, L.; Mameri, S.; Ziessel, R.; Toth, E.; Charbonnière, L. J. *Dalton Trans.* **2009**, 9466–9474.
- (6) (a) Chapman, R. D.; Loda, R. T.; Riehl, J. P.; Schwartz, R. W. *Inorg. Chem.* **1984**, *23*, 1652–1657. (b) Kepert, C. J.; Lu, W.-M.; Semenova, L. J.; Skelton, B. W.; White, A. H. *Aust. J. Chem.* **1999**, *52*, 481–496. (c) Semenova, L. J.; White, A. H. *Aust. J. Chem.* **1999**, *52*, 507–517. (d) Semenova, L. J.; White, A. H. *Aust. J. Chem.* **1999**, *52*, 539–550. (e) Drew, M. G. B.; Iveson, P. B.; Hudson, M. J.; Liljenzin, J. O.; Spjuth, L.; Cordier, P.-Y.; Enarsson, A.; Hill, C.; Madic, C. *J. Chem. Soc., Dalton Trans.* **2000**, 821–830. (f) Drew, M. G. B.; Hudson, M. J.; Iveson, P. B.; Madic, C.; Russel, M. L. *J. Chem. Soc., Dalton Trans.* **2000**, 2711–2720. (g) Mürner, H.-R.; Chassat, E.; Thummel, R. P.; Bünzli, J.-C. G. *J. Chem. Soc., Dalton Trans.* **2000**, 2809–2816. (h) Petit, L.; Daul, C.; Adamo, C.; Maldivi, P. *New J. Chem.* **2007**, *31*, 1738–1745. (i) Hamilton, J. M.; Anhorn, M. J.; Oscarson, K. A.; Reibenspies, J. H.; Hancock, R. D. *Inorg. Chem.* **2011**, *50*, 2764–2770.
- (7) Wu, Q.; Lavigne, J. A.; Tao, Y.; D'Iorio, D.; Wang, S. *Chem. Mater.* **2001**, *13*, 71–77.
- (8) Jäger, M.; Eriksson, L.; Bergquist, J.; Johansson, O. *J. Org. Chem.* **2007**, *72*, 10227–10230.
- (9) Berggren, G.; Huang, P.; Eriksson, L.; Anderlund, M. F. *Appl. Magn. Reson.* **2009**, *36*, 9–24.
- (10) Collins, S. N.; Taylor, S.; Krause, J. A.; Connick, W. B. *Acta Crystallogr.* **2007**, *C63*, m436–m439.
- (11) (a) Abrahamson, M.; Jäger, M.; Osterman, T.; Eriksson, L.; Persson, P.; Becker, H.-C.; Johansson, O.; Hammarström, L. *J. Am. Chem. Soc.* **2006**, *126*, 12616–12617. (b) Jäger, M.; Kumar, R. J.; Göns, H.; Bergquist, J.; Johansson, O. *Inorg. Chem.* **2009**, *48*, 3228–3238. (c) Sharma, S.; Lombeck, F.; Eriksson, L.; Johansson, O. *Chem.—Eur. J.* **2010**, *16*, 7078–7081. (d) Hammarström, L.; Johansson, O. *Coord. Chem. Rev.* **2010**, *254*, 2545–2559.
- (12) Garner, K. L.; Parkes, L. F.; Piper, J. D.; Williams, J. A. G. *Inorg. Chem.* **2010**, *49*, 476–487.
- (13) Baes, C. F. J.; Mesmer, R. E. *Hydrolysis of Cations*; Wiley-Interscience: New York, 1976; Chapter 7, p 129.
- (14) Hamilton, J. M.; Whitehead, J. R.; Williams, N. J.; Ojaimi, M. E.; Thummel, R. P.; Hancock, R. D. *Inorg. Chem.* **2011**, *50*, 3785–3790.
- (15) (a) El-Gahami, M. A.; Ibrahim, S. A.; Fouad, D. M.; Hammam, A. M. *J. Chem. Eng. Data* **2003**, *48*, 29–31. (b) Marie, C.; Miguiditchian, M.; Guillaumont, D.; Tosseng, A.; Berthon, C.; Guilbaud, P.; Duval, M.; Bisson, J.; Guillaneux, D.; Pipelier, M.; Dubreuil, D. *Inorg. Chem.* **2011**, *50*, 6557–6566.
- (16) HypNMR-2008 software: (a) Frassinetti, C.; Ghelli, S.; Gans, P.; Sabatini, A.; Moruzzi, M. S.; Vacca, A. *Anal. Biochem.* **1995**, *231*, 374–382. (b) Frassinetti, C.; Alderighi, L.; Gans, P.; Sabatini, A.; Vacca, A.; Ghelli, S. *Bioanal. Chem.* **2003**, *376*, 1041–1052.
- (17) Lavallee, D. K.; Baughman, M. D.; Phillips, M. D. *J. Am. Chem. Soc.* **1977**, *99*, 718–724.
- (18) (a) Nakamoto, K. *J. Phys. Chem.* **1960**, *64*, 1420–1425. (b) Bessel, C. A.; See, R. F.; Jameson, D. L.; Churchill, M. R.; Takeuchi, K. J. *J. Chem. Soc., Dalton Trans.* **1992**, 3223–3228. (c) Bowes, K. F.; Clark, I. P.; Cole, J. M.; Gourlay, M.; Griffin, M. E.; Mahon, M. F.; Ooi, L.; Parker, A. W.; Raithby, P. R.; Sparkesc, H. A.; Towrie, M. *Cryst. Eng. Commun.* **2005**, *7*, 269–275.
- (19) Göller, A. H.; Grummt, U.-W. *Chem. Phys. Lett.* **2002**, *354*, 233–242.
- (20) Hergold-Brundic, A.; Popovic, Z.; Matkovic-Calogovoc, D. *Acta Crystallogr.* **1996**, *CS2*, 3154–3157.
- (21) (a) Kepert, C. J.; Skelton, B. W.; White, A. H. *Aust. J. Chem.* **1994**, *47*, 391–396. (b) Drew, M. G. B.; Hudson, M. J.; Iveson, P. B.; Russell, M. L.; Liljenzin, J.-O.; Skalberg, M.; Spjuth, L.; Madic, C. *J. Chem. Soc., Dalton Trans.* **1998**, 2973–2980. (c) Berthon, C.; Grigoriev, M. S. *Acta Crystallogr.* **2005**, *E61*, o1216–o1217.
- (22) Bazzicalupi, C.; Bencini, A.; Bianchi, A.; Danesi, A.; Faggi, E.; Giorgi, C.; Santarelli, S.; Valtancoli, B. *Coord. Chem. Rev.* **2008**, *285*, 1052–1068.
- (23) For a forced coplanar trans-trans arrangement of the three aromatic rings in **L3**, we calculate a H(py)…N(quinoline) contact distance of 1.94 Å, a value much shorter than the sum of the van der Waals radii (1.46 + 1.06 = 2.52 Å). Bondi, A. *J. Phys. Chem.* **1964**, *68*, 441–451.
- (24) All hydrogen atoms were observed from the difference Fourier map and refined without constraints except for **4**, where restraints on the bond lengths and bond angles were applied for aromatic hydrogen atoms connected to carbon atoms, but the additional hydrogen atom bound to nitrogen atom was freely refined.
- (25) The nature of the hydrogen-bound counteranions has only a minor effect on the conformation of the protonated cations, as exemplified by the almost superimposable molecular structures of $[HL_2]^+$ in **1** and $[HL_2](FeCl_4)^{10-}$ (Figure S11 in the SI) and for $[H_2L_2]^{2+}$ in **2** and $[H_2L_2]I_2$ (**5**; Figure S12 in the SI).
- (26) (a) Hamacek, J.; Borkovec, M.; Piguet, C. *Chem.—Eur. J.* **2005**, *11*, 5227–5237. (b) Hamacek, J.; Borkovec, M.; Piguet, C. *Chem.—Eur. J.* **2005**, *11*, 5217–5226. (c) Hamacek, J.; Borkovec, M.; Piguet, C. *Dalton Trans.* **2006**, 1473–1490. (d) Piguet, C. *Chem. Commun.* **2010**, *46*, 6209–6231.
- (27) Ercolani, G.; Piguet, C.; Borkovec, M.; Hamacek, J. *J. Phys. Chem. B* **2007**, *111*, 12195–12203.
- (28) Ercolani, G.; Schiaffino, L. *Angew. Chem., Int. Ed.* **2011**, *50*, 1762–1768.
- (29) Wulfsberg, G. *Inorganic Chemistry*; University Science Books: Sausalito, CA, 2000; Chapter 2.
- (30) Song, D.; Wu, Q.; Hook, A.; Kozin, I.; Wang, S. *Organometallics* **2001**, *20*, 4683–4689.
- (31) Zhao, Q.-L.; Li, G.-P. *Acta Crystallogr.* **2009**, *E65*, m693.
- (32) (a) Piguet, C.; Bochet, C. G.; Williams, A. F. *Helv. Chim. Acta* **1993**, *76*, 372–384. (b) Constable, E. C.; Baum, G.; Bill, E.; Dyson, R.; van Eldik, R.; Fenske, D.; Kaderli, S.; Morris, D.; Neubrand, A.; Neuburger, M.; Smith, D. R.; Wieghardt, K.; Zehnder, M.; Zuberbühler, A. D. *Chem.—Eur. J.* **1999**, *5*, 498–508.
- (33) Desreux, J. F. In *Lanthanide Probes in Life, Chemical and Earth Sciences*; Bünzli, J.-C. G., Choppin, G. R., Eds.; Elsevier: Amsterdam, The Netherlands, 1989; Chapter 2, p 43.
- (34) Izod, K.; Liddle, S. T.; Clegg, W. *Inorg. Chem.* **2004**, *43*, 214–218.
- (35) Altomare, A.; Burla, M. C.; Camalli, M.; Cascarano, G.; Giacovazzo, C.; Guagliardi, A.; Moliterni, G.; Polidori, G.; Spagna, R. *J. Appl. Crystallogr.* **1999**, *32*, 115–119.
- (36) Sheldrick, G. M. *SHELXL97: Program for the Solution and Refinement of Crystal Structures*; University of Göttingen: Göttingen, Germany, 1997.
- (37) ORTEP3 for Windows: Farrugia, L. J. *J. Appl. Crystallogr.* **1997**, *30*, 565.

Protonation and Complexation Properties of Polyaromatic Terdentate Six-Membered Chelate Ligands.

Thi Nhu Y Hoang, Timothée Lathion, Laure Guénée, Emmanuel Terazzi and Claude Piguet*

Supporting Information

(38 pages)

Appendix 1. Derivation of eqn (4).



The application of the law of mass action for equilibria (1)-(3) gives (standard concentration of the reference state $c^0 = 1 \text{ M}$):

$$K_a^1 = \frac{|\text{Eu(OH)}||\text{H}|}{|\text{Eu}||\text{H}_2\text{O}|} \quad (\text{S1})$$

$$\beta_{1,0,1}^{\text{Eu,H,Lk}} = \frac{|\text{Eu(Lk)}|}{|\text{Eu}||\text{Lk}|} \quad (\text{S2})$$

$$\beta_{0,1,1}^{\text{Eu,H,Lk}} = \frac{|\text{HLk}|}{|\text{H}||\text{Lk}|} \quad (\text{S3})$$

The ratio of the two formation constants modeling the competition between Eu^{3+} (eq nS2) and H^+ (eqn S3) for complexing **Lk** can be written as

$$\frac{\beta_{1,0,1}^{\text{Eu,H,Lk}}}{\beta_{0,1,1}^{\text{Eu,H,Lk}}} = \frac{|\text{Eu(Lk)}|}{|\text{HLk}|} \cdot \frac{|\text{H}|}{|\text{Eu}|} \quad (\text{S4})$$

Introducing eqn (S1) into eqn (S4) yields

$$\frac{\beta_{1,0,1}^{\text{Eu,H,Lk}}}{\beta_{0,1,1}^{\text{Eu,H,Lk}}} = \frac{|\text{Eu(Lk)}|}{|\text{HLk}|} \cdot \frac{K_a^1 |\text{H}_2\text{O}|}{|\text{Eu(OH)}|} \quad (\text{S5})$$

The consideration of the mass balance for water in organic solvent (eqn S6), followed by its introduction into eqn (S5) eventually yields eqn (S7), which is easily re-arranged into the target ratio of eqn (4).

$$|\text{H}_2\text{O}|_{\text{tot}} = |\text{H}_2\text{O}| + |\text{Eu(OH)}| \quad (\text{S6})$$

$$\frac{\beta_{1,0,1}^{\text{Eu,H,Lk}}}{\beta_{0,1,1}^{\text{Eu,H,Lk}}} = \frac{|\text{Eu(Lk)}|}{|\text{HLk}|} \cdot \frac{K_a^1 |\text{H}_2\text{O}|}{(|\text{H}_2\text{O}|_{\text{tot}} - |\text{H}_2\text{O}|)} \quad (\text{S7})$$

$$\frac{|\text{Eu(Lk)}|}{|\text{HLk}|} = \frac{\beta_{1,0,1}^{\text{Eu,H,Lk}}}{\beta_{0,1,1}^{\text{Eu,H,Lk}}} \cdot \frac{(|\text{H}_2\text{O}|_{\text{tot}} - |\text{H}_2\text{O}|)}{K_a^1 |\text{H}_2\text{O}|} \quad (4)$$

Appendix 2. Speciation obtained from ^1H NMR titrations of L2 with $\text{Zn}(\text{CF}_3\text{SO}_3)_2$.

For a given stoichiometric $|\text{Zn}|_{\text{tot}} / |\text{L2}|_{\text{tot}}$ ratio, the integrated intensities of the ^1H NMR signals recorded for the same proton in **L2** (I_L), $[\text{Zn}(\text{L2})]^{2+}$ ($I_{\text{Zn-L}}$) and $[\text{Zn}(\text{L2})_2]^{2+}$ ($I_{\text{Zn-2L}}$) can be combined and scaled with respect to $[\text{Zn}(\text{L2})]$ with eqns (S8)-(S9).

$$|\text{L2}| = \left(\frac{I_L}{I_{\text{Zn-L}}} \right) [\text{Zn}(\text{L2})] \quad (\text{S8})$$

$$[\text{Zn}(\text{L2})_2] = \left(\frac{I_{\text{Zn-2L}}}{2I_{\text{Zn-L}}} \right) [\text{Zn}(\text{L2})] \quad (\text{S9})$$

Introducing eqns (S8)-(S9) into the mass balance eqn (S10) yields eqn (S11) after straightforward algebraic transformations.

$$|\text{L2}|_{\text{tot}} = |\text{L2}| + [\text{Zn}(\text{L2})] + 2[\text{Zn}(\text{L2})_2] \quad (\text{S10})$$

$$[\text{Zn}(\text{L2})] = |\text{L2}|_{\text{tot}} \left(\frac{I_{\text{Zn-L}}}{I_L + I_{\text{Zn-L}} + I_{\text{Zn-2L}}} \right) \quad (\text{S11})$$

Introducing eqn (S11) into eqns (S8)-(S9) gives the speciation of the free ligand (eqn S12) and of $[\text{Zn}(\text{L2})_2]^{2+}$ (eqn S13).

$$|\text{L2}| = |\text{L2}|_{\text{tot}} \left(\frac{I_L}{I_L + I_{\text{Zn-L}} + I_{\text{Zn-2L}}} \right) \quad (\text{S12})$$

$$[\text{Zn}(\text{L2})_2] = \frac{|\text{L2}|_{\text{tot}}}{2} \left(\frac{I_{\text{Zn-2L}}}{I_L + I_{\text{Zn-L}} + I_{\text{Zn-2L}}} \right) \quad (\text{S13})$$

The missing concentration $|\text{Zn}|$ (eqn S15) can be deduced from the mass balance written for the metal concentrations (eqn S14).

$$|\text{Zn}| = |\text{Zn}|_{\text{tot}} - [\text{Zn}(\text{L2})] - [\text{Zn}(\text{L2})_2] \quad (\text{S14})$$

$$|\text{Zn}| = |\text{Zn}|_{\text{tot}} - \frac{|\text{L2}|_{\text{tot}}}{2} \left(\frac{2I_{\text{Zn-L}} + I_{\text{Zn-2L}}}{I_L + I_{\text{Zn-L}} + I_{\text{Zn-2L}}} \right) \quad (\text{S15})$$

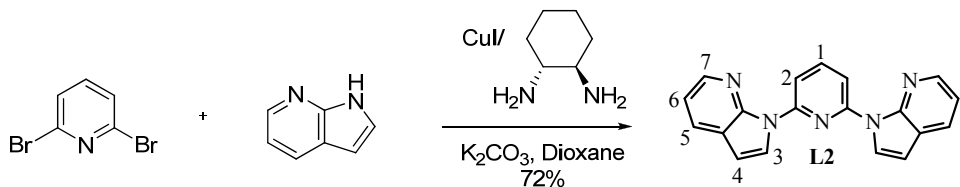
The final introduction of these concentrations (eqns (S11)-(S13) and (S15)) into the laws of mass action associated with equilibrium (15) and (16) yields eq (S16) and (S17), respectively (the standard concentration of the reference state is set at 1 M).

$$\beta_{1,1}^{\text{Zn,L2}} = \frac{[\text{Zn}(\text{L2})]}{|\text{Zn}| \cdot |\text{L2}|} = \frac{I_{\text{Zn-L}}}{I_L} \left(\frac{I_L + I_{\text{Zn-L}} + I_{\text{Zn-2L}}}{|\text{Zn}|_{\text{tot}} (I_L + I_{\text{Zn-L}} + I_{\text{Zn-2L}}) - |\text{L2}|_{\text{tot}} (I_{\text{Zn-L}} + I_{\text{Zn-2L}})} \right) \quad (\text{S16})$$

$$\beta_{1,2}^{\text{Zn,L2}} = \frac{[\text{Zn}(\text{L2})_2]}{|\text{Zn}| \cdot |\text{L2}|^2} = \frac{I_{\text{Zn-2L}}}{(I_L)^2 |\text{L2}|_{\text{tot}}} \left(\frac{(I_L + I_{\text{Zn-L}} + I_{\text{Zn-2L}})^2}{2|\text{Zn}|_{\text{tot}} (I_L + I_{\text{Zn-L}} + I_{\text{Zn-2L}}) - |\text{L2}|_{\text{tot}} (2I_{\text{Zn-L}} + I_{\text{Zn-2L}})} \right) \quad (\text{S17})$$

Appendix 3. Preparation of the ligands and complexes.

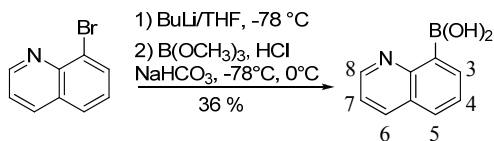
Preparation of 2,6-bis(azaindol-yl)pyridine (**L2**).



2,6-dibromopyridine (200 mg, 0.84 mmol), 7-azaindole (300 mg, 2.53 mmol), K_2CO_3 (707 mg, 5.07 mmol), trans-1,2-diaminocyclohexane (29 mg, 0.25 mmol) and CuI (8 mg, 0.042 mmol) in dioxane was degassed with N_2 for 30 min. The mixture was then refluxed under an inert atmosphere for 72 h. The solvent was evaporated and the resulting a brown residue was extracted with CH_2Cl_2 (3x25 mL) and washed with water (50 mL). The organic layer was dried over MgSO_4 and the solvent was evaporated under reduced pressure. The resulting solid was carefully washed with acetonitrile to give 189 mg of **L2** (0.60 mmol, yield = 72%) as a white solid.

^1H NMR (CDCl_3 , 400 MHz): δ 8.83 (d, 2H, $^3J = 8$ Hz, H2); 8.47 (d, 2H, $^3J = 4$ Hz, H3); 8.44 (dd, 2H, $^3J = 4$ Hz, $^4J = 1.6$ Hz, H7); 8.06 (t, 1H, $^3J = 8$ Hz, H1); 7.99 (dd, 2H, $^3J = 8$ Hz, $^4J = 1.6$ Hz, H5); 7.20 (dd, 2H, $^3J = 8$ Hz, $^4J = 4.6$ Hz, H6); 6.68 (d, 2H, $^3J = 8$ Hz, H4). ^{13}C NMR (CDCl_3 , 100 MHz): δ 149.1 (C_{quat}); 147.8 (C_{quat}); 143.7 (C7); 140.6 (C1); 129.14 (C5); 126.4 (C3); 123.6 (C_{quat}); 117.3 (C6); 111.4 (C2); 102.4 (C4). ESI-MS: m/z : 313.3 [M+H]⁺, 623.5 [2M+H]⁺; calcd for $\text{C}_{19}\text{H}_{13}\text{N}_5$: 312.1249.

Preparation of 8-quinolineboronic acid.

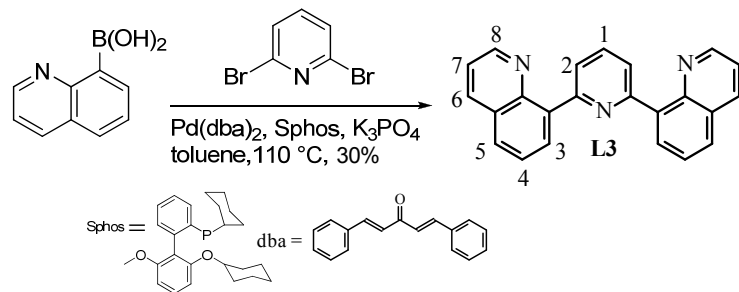


8-bromoquinoline (1 g, 4.8 mmol) in THF (5 mL) was cooled to -78 °C under N_2 and *n*-butyllithium (1.55 M in hexane, 3.6 mL, 5.76 mmol) was then added dropwise. After 1 h, trimethyl borate (1.2 mL, 10.56 mmol) was added dropwise, and the mixture was allowed to reach RT. After stirring for one more hour, HCl (2 M, 20 mL) was added and the resulting layer was washed with Et_2O (30 mL)

and neutralized with solid NaHCO₃. The resulting light brown precipitate was collected and crystallized from acetone/hexane to give 310 mg of 8-quinolineboronic acid (1.73 mmol, yield = 36%) as a pale yellow solid.

¹H NMR (MeOD, 400 MHz): δ 9.27 (dd, 1H, ³J = 5.3 Hz, ⁴J = 1.7 Hz, H8); 8.48 (dd, 1H, ³J = 8.3 Hz, ⁴J = 1.6 Hz, H6); 8.07 (dd, 1H, ³J = 6.8 Hz, ⁴J = 1.5 Hz, H5); 7.76 (dd, 1H, ³J = 8.2 Hz, ⁴J = 1.4 Hz, H3); 7.66 (dd, 1H, ³J = 8.3 Hz, ³J = 5.3 Hz, H7); 7.55 (dd, 1H, ³J = 8.2 Hz, ³J = 6.9 Hz, H4). ESI-MS: *m/z* : 156.1 [M-OH]⁺; calcd for C₉H₈BNO₂: 173.06.

Preparation of 2,6-bis(8-quinolin-yl)pyridine (L3).



2,6-dibromopyridine (187 mg, 0.8 mmol), K₃PO₄ (1.6 g, 7.11 mmol), 8-quinolineboronic acid (274 mg, 1.58 mmol) and Sphos (13 mg, 0.03 mmol) in toluene (5 mL) was degassed with N₂ for 30 min. Pd(dba)₂ (18 mg, 0.03 mmol) was added and the mixture heated at 150 °C under an inert atmosphere for 15 h. After cooling, CH₂Cl₂ (15 mL) was added and the insoluble residue was removed by filtration. Evaporation of the filtrate followed by purification by column chromatography (CH₂Cl₂/MeOH: 97.5/2.5) yielded 80 mg of L3 (0.24 mmol, yield = 30%) as a white solid.

¹H NMR (CDCl₃, 400 MHz): δ 9.03 (dd, 2H, ³J = 4.0 Hz, ⁴J = 1.6 Hz, H8); 8.30 (dd, 2H, ³J = 7.2 Hz, ⁴J = 1.2 Hz, H3); 8.26 (dd, 2H, ³J = 8.4 Hz, ⁴J = 1.6 Hz, H6); 8.14 (d, 2H, ³J = 8.0 Hz, H2); 7.97 (t, 1H, ³J = 7.2 Hz, H1); 7.91 (dd, 2H, ³J = 8.0 Hz, ⁴J = 1.2 Hz, H5); 7.69 (dd, 2H, ³J = 8.4 Hz, ⁴J = 7.6 Hz, H4); 7.48 (dd, 2H, ³J = 8.4 Hz, ⁴J = 4.4 Hz, H7). ¹³C NMR (CDCl₃, 100 MHz): δ 156.7 (C_{quat}); 150.2 (C8); 146.1 (C_{quat}); 139.5 (C6); 136.4 (C_{quat}); 134.8(C1); 131.6 (C3); 128.7 (C_{quat}); 128.5 (C5); 126.6 (C4); 125.5 (C2); 120.9 (C7). ESI-MS: *m/z*: 333.5 [M+H]⁺, *m/z*: 667.5 [2M+H]⁺; calcd for C₂₃H₁₅N₃: 333.12.

Preparation of YI₃(THF)_{3.5}.³⁴ All manipulation were carried out under an atmosphere of dry argon using either standard Schlenk techniques or a glovebox where the water and oxygen levels were monitored (<1 ppm). THF was freshly distilled under argon from sodium/benzophenone, petroleum ether was distilled under argon from CaH₂. THF and petroleum ether were always carefully degassed before use. Elemental iodine (4.26 g, 16.9 mmol) was added under argon to a suspension of yttrium powder (1 g, 11.2 mmol) in degassed anhydrous THF (10 mL) at 0°C. The ice bath was removed and the solution stirred for 3.5 days at RT. Petroleum ether (fraction 30-60, 50 ml) was added to the dark mixture and the precipitated brown solid was filtered, washed with petroleum ether (2x30 ml) and heated under vacum (130 °C, 10 Torr) for 6 h in order to sublime the excess of iodine. The resulting light brown solid was purified by Soxhlet extraction with degassed anhydrous THF (200 mL) for 3 days to give YI₃(THF)_{3.5} as a light brown solid.

Table S1 ^1H NMR Chemical Shifts Computed for **L k** , $[\text{HL}\mathbf{k}]^+$, $[\text{H}_2\text{L}\mathbf{k}]^{2+}$ ($k = 1\text{-}3$), $[\text{Zn}(\mathbf{L}2)_n]^{2+}$ ($n = 1\text{-}2$) and $[\text{Y}(\mathbf{L}2)]^{3+}$ in $\text{CD}_3\text{CN}/\text{CDCl}_3$ (1:1) at 298 K.

Ligand	H1	H2	H3	H4	H5	H6	H7	H8
L1	8.00	8.45	8.64	7.92	7.40	8.69	-	-
$[\text{HL1}]^+$	8.35	8.57	9.09	8.52	7.95	8.99	-	-
$[\text{H}_2\text{L1}]^{2+}$	8.51	8.63	8.12	8.83	8.25	9.17	-	-
L2	8.10	8.86	8.51	6.73	8.03	7.23	8.41	-
$[\text{HL2}]^+$	8.16	7.54	8.16	7.01	8.45	7.61	8.89	-
$[\text{H}_2\text{L2}]^{2+}$	8.44	7.84	8.22	7.22	8.84	7.75	8.37	-
$[\text{Zn}(\mathbf{L}2)]^{2+}$	8.30	7.70	8.07	7.06	8.45	7.60	8.70	-
$[\text{Zn}(\mathbf{L}2)_2]^{2+}$	8.28	7.53	7.65	6.69	7.99	7.08	8.05	-
$[\text{Y}(\mathbf{L}2)]^{3+}$ ^a	8.30	7.57	7.90	7.11	8.48	7.68	9.15	-
L3	7.94	8.12	8.25	7.70	7.96	8.32	7.51	8.97
$[\text{HL3}]^+$	8.24	8.38	9.20	8.41	8.72	9.37	8.17	8.41
$[\text{H}_2\text{L3}]^{2+}$	8.95	8.45	8.59	8.20	8.58	9.30	8.18	9.12

^a in pure CD_2Cl_2 .

Table S2 Summary of Crystal Data, Intensity Measurements and Structure Refinements for $[\text{HL2}](\text{CF}_3\text{SO}_3)$ (**1**), $[\text{H}_2\text{L2}](\text{CF}_3\text{SO}_3)_2$ (**2**), $[\text{HL3}](\text{CF}_3\text{SO}_3)$ (**3**), $[\text{H}_2\text{L3}](\text{CF}_3\text{SO}_3)_2$ (**4**) and $[\text{H}_2\text{L2}]\text{I}_2$ (**5**).

	1	2	3	4	5
Empirical formula	$\text{C}_{20}\text{H}_{14}\text{F}_3\text{N}_5\text{O}_3\text{S}$	$\text{C}_{21}\text{H}_{15}\text{F}_6\text{N}_5\text{O}_6\text{S}_2$	$\text{C}_{24}\text{H}_{16}\text{F}_3\text{N}_3\text{O}_3\text{S}$	$\text{C}_{25}\text{H}_{17}\text{F}_6\text{N}_3\text{O}_6\text{S}_2$	$\text{C}_{19}\text{H}_{15}\text{I}_2\text{N}_5$
Formula weight	461.42	611.50	483.46	633.54	567.16
Temperature	180(2)K	180(2)K	180(2)K	180(2)K	293(2)K
Wavelength	1.54184 Å	1.51484 Å	1.54184 Å	1.54184 Å	1.54184 Å
Crystal System, Space group	Monoclinic, $C\ 2/c$	Triclinic, $P\ -1$	Triclinic, $P\ -1$	Monoclinic, $P\ 2_1/c$	Monoclinic, $C\ 2/c$
Unit cell dimensions	$a = 24.5529(5)$ Å $b = 6.63776(11)$ Å $c = 24.3027(5)$ Å $\alpha = 90^\circ$ $\beta = 106.189(2)^\circ$. $\gamma = 90^\circ$	$a = 9.0329(9)$ Å $b = 11.1765(10)$ Å $c = 13.5512(12)$ Å $\alpha = 113.068(9)^\circ$ $\beta = 99.997(8)^\circ$. $\gamma = 101.089(8)^\circ$	$a = 7.3518(3)$ Å $b = 10.5566(4)$ Å $c = 14.0959(6)$ Å $\alpha = 100.942(3)^\circ$ $\beta = 100.918(3)^\circ$. $\gamma = 94.309(3)^\circ$	$a = 9.52829(13)$ Å $b = 9.93085(13)$ Å $c = 27.9290(4)$ Å $\alpha = 90^\circ$ $\beta = 102.9336(14)^\circ$. $\gamma = 90^\circ$	$a = 14.4182(2)$ Å $b = 10.50522(13)$ Å $c = 13.8850(3)$ Å $\alpha = 90^\circ$ $\beta = 111.170(2)^\circ$. $\gamma = 90^\circ$
Volume in Å ³	3803.70(15)	1187.30(19)	1047.62(7)	2575.70(6)	1961.17(6)
Z, Calculated density	8, 1.612 Mg/m ³	2, 1.710 Mg/m ³	2, 1.533 Mg/m ³	4, 1.634 Mg/m ³	4, 1.921 Mg/m ³
Absorption coefficient	2.113 mm ⁻¹	2.950 mm ⁻¹	1.921 mm ⁻¹	2.722 mm ⁻¹	25.288 mm ⁻¹
$F(000)$	1888	620	496	1288	1080
Theta range for data collection	3.75 to 74.04 °	3.6852 to 73.5001 °	3.26 to 73.40 °	3.25 to 73.41 °	5.34 to 73.30 °
Limiting indices	-28≤ h ≤30,	-11≤ h ≤7,	-9≤ h ≤5,	-11≤ h ≤11,	-17≤ h ≤17,

	$-6 \leq k \leq 8,$ $-30 \leq l \leq 30$	$-13 \leq k \leq 13,$ $-16 \leq l \leq 16$	$-12 \leq k \leq 13,$ $-16 \leq l \leq 17$	$-12 \leq k \leq 8,$ $-26 \leq l \leq 34$	$-12 \leq k \leq 12,$ $-17 \leq l \leq 15$
Reflections collected / unique	13809 / 3790 [$R(\text{int}) = 0.0346$]	7528 / 4614 [$R(\text{int}) = 0.0495$]	6749 / 4070 [$R(\text{int}) = 0.0144$]	14578 / 5036 [$R(\text{int}) = 0.0729$]	6212 / 1934 [$R(\text{int}) = 0.0301$]
Completeness to theta	74.04° / 97.9%	73.66° / 96.2 %	73.40° / 96.4 %	68.00° / 99.9 %	66.97° / 99.9 %
Data / restraints / parameters	3790 / 0 / 332	4614 / 0 / 421	4070 / 0 / 371	5036 / 0 / 387	1934 / 0 / 123
Goodness-of-fit on F^2	1.005	1.089	1.054	1.031	1.055
Final R indices [$I > 2\sigma(I)$]	$R_1 = 0.0448,$ $\omega R_2 = 0.1208$	$R_1 = 0.0726,$ $\omega R_2 = 0.2005$	$R_1 = 0.0479,$ $\omega R_2 = 0.1399$	$R_1 = 0.0484,$ $\omega R_2 = 0.1379$	$R_1 = 0.0330,$ $\omega R_2 = 0.0916$
R indices (all data)	$R_1 = 0.0550,$ $\omega R_2 = 0.1319$	$R_1 = 0.0888,$ $\omega R_2 = 0.2213$	$R_1 = 0.0511,$ $\omega R_2 = 0.1437$	$R_1 = 0.0519,$ $\omega R_2 = 0.1426$	$R_1 = 0.0342,$ $\omega R_2 = 0.0933$
Largest diff. peak and hole	0.395 and -0.327 $e \cdot \text{\AA}^{-3}$	0.624 and -0.690 $e \cdot \text{\AA}^{-3}$	0.955 and -0.528 $e \cdot \text{\AA}^{-3}$	0.502 and -0.472 $e \cdot \text{\AA}^{-3}$	0.861 and -0.535 $e \cdot \text{\AA}^{-3}$

Table S3 Selected Bond Distances (Å), Bond Angles (°) in [HL2](CF₃SO₃) (**1**).^a

Bond Distances (Å)					
Atom 1	Atom 2	Distance	Atom 1	Atom 2	Distance
N3	C8	1.332(3)	N3	C12	1.327(3)
N2	C8	1.411(3)	N4	C12	1.411(3)
N2	C7	1.391(3)	N4	C19	1.372(3)
N1	C7	1.336(3)	N5	C19	1.339(3)

Angles (°)							
Atom 1	Atom 2	Atom 3	Angle	Atom 1	Atom 2	Atom 3	Angle
N3	C8	N2	115.59(17)	N3	C12	N4	114.33(17)
C8	N2	C7	129.03(17)	C12	N4	C19	127.28(17)
N2	C7	N1	127.54(18)	N4	C19	N5	128.66(18)

^a Numbering scheme in Fig. S7

Table S4 Selected Least-Squares Planes Data for [HL2](CF₃SO₃) (**1**).^a

Least-Squares Planes			
Least-squares planes description	Abbreviation	Max. deviation/Å	Atom
Azaindole 1	Az1		
C1 C2 C3 C4 C5 C6 N2 C7 N1		0.006(1)	N1
Pyridine	Py		
N3 C8 C9 C10 C11 C12		-0.004(1)	C9
Azaindole 2	Az2		
C13 C14 C15 C16 C17 C18 N5 C19 N4		-0.008(1)	C19

^a Numbering scheme in Fig. S7

Interplanar angles (°) (esd < 0.1°)

	Py	Az2
Az1	4.2	0.8
Py		3.7

Table S5 Hydrogen bonds in $[\text{HL2}](\text{CF}_3\text{SO}_3)$ (**1**).^a

D-H···A	d(D-H)/Å	d(H···A)/Å	d(D···A)/Å	$\angle(\text{DHA})/^\circ$
N(5)-H(5)···N(1)	0.92(3)	1.98(3)	2.849(2)	157(3)
N(5)-H(5)···N(3)	0.92(3)	2.18(3)	2.734(2)	117(2)

^a Numbering scheme in Fig. S7

Table S6 Selected Bond Distances (Å), Bond Angles (°) in $[\text{H}_2\text{L2}](\text{CF}_3\text{SO}_3)_2$ (**2**).^a

Bond Distances (Å)					
Atom 1	Atom 2	Distance	Atom 1	Atom 2	Distance
N3	C8	1.327(5)	N3	C12	1.334(5)
N2	C8	1.411(3)	N4	C12	1.406(5)
N2	C7	1.360(5)	N4	C19	1.364(5)
N1	C7	1.321(5)	N5	C19	1.346(5)

Angles (°)			
Atom 1	Atom 2	Atom 3	Angle
N3	C8	N2	114.7(3)
C8	N2	C7	126.6(3)
N2	C7	N1	128.4(3)
N3	C12	N4	114.8(3)
C12	N4	C19	126.8(3)
N4	C19	N5	128.5(4)

^a Numbering scheme in Fig. S7

Table S7 Selected Least-Squares Planes Data for $[H_2\mathbf{L}2](CF_3SO_3)_2$ (**2**).^a

Least-Squares Planes

Least-squares planes description	Abbreviation	Max. deviation/ \AA	Atom
Azaindole 1 C1 C2 C3 C4 C5 C6 N2 C7 N1	Az1	0.04(1)	C7
Pyridine N3 C8 C9 C10 C11 C12	Py	0.02(1)	C8
Azaindole 2 C13 C14 C15 C16 C17 C18 N5 C19 N4	Az2	0.04(1)	C14

^a Numbering scheme in Fig. S7

Interplanar angles ($^{\circ}$) (esd < 0.1°)

	Py	Az2
Az1	31.7	22.9
Py		20.9

Table S8 Hydrogen bonds in $[H_2\mathbf{L}2](CF_3SO_3)_2$ (**2**).^a

D-H \cdots A	d(D-H)/ \AA	d(H \cdots A)/ \AA	d(D \cdots A)/ \AA	\angle (DHA)/ $^{\circ}$
N(1)-H(1A) \cdots O(4) ^{# b}	0.91(5)	1.89(5)	2.770(4)	163(4)
N(1)-H(1A) \cdots N(3)	0.91(5)	2.45(5)	2.840(5)	106(3)
N(5)-H(5A) \cdots O(4) ^{§ b}	0.90(5)	1.99(4)	2.796(5)	147(4)
N(5)-H(5A) \cdots N(3)	0.90(5)	2.30(4)	2.783(5)	114(3)

^a Numbering scheme in Fig. S7. ^b Symmetry transformation used to generate equivalent atoms:

#: $-x+1, -y+2, -z+1$; §: $x, y-1, z$.

Table S9 Selected Bond Distances (Å), Bond Angles (°) in [HL3](CF₃SO₃) (**3**).^a

Bond Distances (Å)					
Atom 1	Atom 2	Distance	Atom 1	Atom 2	Distance
N2	C10	1.358(2)	N2	C14	1.358(2)
C10	C8	1.485(3)	C14	C15	1.482(3)
C8	C9	1.427(3)	C15	C23	1.431(3)
N1	C9	1.362(3)	N3	C23	1.368(2)

Angles (°)							
Atom 1	Atom 2	Atom 3	Angle	Atom 1	Atom 2	Atom 3	Angle
N2	C10	C8	120.30(17)	N2	C14	C15	119.12(16)
C10	C8	C9	123.33(17)	C14	C15	C23	123.30(16)
C8	C9	N1	118.90(17)	C15	C23	N3	119.47(17)

^a Numbering scheme in Fig. S8

Table S10 Selected Least-Squares Planes Data for [HL3](CF₃SO₃) (**3**).^a

Least-Squares Planes			
Least-squares planes description	Abbreviation	Max. deviation/Å	Atom
Quinoline 1	Qui1		
N1 C1 C2 C3 C4 C5 C6 C7 C8 C9		-0.018	C7
Pyridine	Py		
N2 C10 C11 C12 C13 C14		0.011	N2
Quinoline 2	Qui2		
C15 C16 C17 C18 C19 C20 C21 C22 N3 C23		0.012	C21

^a Numbering scheme in Fig. S8

Interplanar angles (°) (esd < 0.1°)

	Py	Qui2
Qui1	32.1	33.7
Py		3.4

Table S11 Hydrogen bonds in $[\text{HL3}](\text{CF}_3\text{SO}_3)$ (**3**).^a

D-H···A	d(D-H)/Å	d(H···A)/Å	d(D···A)/Å	$\angle(\text{DHA})/^\circ$
N(2)-H(2)···N(1)	0.88(3)	2.25(3)	2.790(2)	119(2)
N(2)-H(2)···N(3)	0.88(3)	1.87(3)	2.609(2)	141(2)

^a Numbering scheme in Fig. S8.

Table S12 Selected Bond Distances (Å), Bond Angles (°) in $[\text{H}_2\text{L3}](\text{CF}_3\text{SO}_3)_2$ (**4**).^a

Bond Distances (Å)					
Atom 1	Atom 2	Distance	Atom 1	Atom 2	Distance
N2	C10	1.343(3)	N2	C14	1.348(3)
C10	C8	1.485(3)	C14	C15	1.485(3)
C8	C9	1.421(3)	C15	C23	1.427(3)
N1	C9	1.373(3)	N3	C23	1.371(3)

Angles (°)							
Atom 1	Atom 2	Atom 3	Angle	Atom 1	Atom 2	Atom 3	Angle
N2	C10	C8	117.33(18)	N2	C14	C15	117.45(18)
C10	C8	C9	123.45(19)	C14	C15	C23	122.87(18)
C8	C9	N1	122.28(18)	C15	C23	N3	121.94(18)

^a Numbering scheme in Fig. S8

Table S13 Selected Least-Squares Planes Data for $[H_2\mathbf{L3}](CF_3SO_3)_2$ (**4**).^a

Least-Squares Planes			
Least-squares planes description	Abbreviation	Max. deviation/ \AA	Atom
Quinoline 1 N1 C1 C2 C3 C4 C5 C6 C7 C8 C9	Qui1	-0.029(1)	C3
Pyridine N2 C10 C11 C12 C13 C14	Py	0.021(1)	C10
Quinoline 2 C15 C16 C17 C18 C19 C20 C21 C22 N3 C23	Qui2	0.044(1)	N3

^a Numbering scheme in Fig. S8

Interplanar angles ($^\circ$) (esd < 0.1°)

	Py	Qui2
Qui1	31.6	42.2
Py		23.9

Table S14 Hydrogen bonds in $[H_2\mathbf{L3}](CF_3SO_3)_2$ (**4**).^a

D-H \cdots A	d(D-H)/ \AA	d(H \cdots A)/ \AA	d(D \cdots A)/ \AA	\angle (DHA)/ $^\circ$
N(1)-H(1) \cdots N(2)	0.86(3)	2.15(3)	2.790(2)	131(3)
N(3)-H(3) \cdots N(2)	0.88(3)	2.13(3)	2.721(2)	130(2)
N(3)-H(3) \cdots O(1T)	0.81(3)	2.28(3)	2.870(2)	131(2)

^a Numbering scheme in Fig. S8.

Table S15 Selected Bond Distances (\AA), Bond Angles ($^\circ$) in $[\text{H}_2\text{L}2]\text{I}_2$ (**2**).^b

Bond Distances (\AA)		
Atom 1	Atom 2	Distance
N3	C8	1.319(4)
N2	C8	1.415(5)
N2	C7	1.369(5)
N1	C7	1.332(6)

Angles ($^\circ$)			
Atom 1	Atom 2	Atom 3	Angle
N3	C8	N2	115.0(3)
C8	N2	C7	126.6(3)
N2	C7	N1	128.7(4)

^a Numbering scheme in Fig. S13

Table S16 Selected Least-Squares Planes Data for $[\text{H}_2\text{L}2]\text{I}_2$ (**5**).^a

Least-Squares Planes			
Least-squares planes description	Abbreviation	Max. deviation/ \AA	Atom
Azaindole 1	Az1		
C1 C2 C3 C4 C5 C6 N2 C7 N1		0.04(1)	C7
Pyridine	Py		
N3 C8 C9 C10 C11 C12		0.01(1)	C8

^a Numbering scheme in Fig. S13

Interplanar angles ($^\circ$) (esd < 0.1°)

	Py	Az1'
Az1	26.6	34.8
Py		26.6

Table S17 Hydrogen bonds in $[H_2\mathbf{L}2]I_2$ (**5**).^a

D-H···A	d(D-H)/Å	d(H···A)/Å	d(D···A)/Å	$\angle(DHA)^\circ$
N(1)-H(1)···N(3)	0.81(6)	2.41(5)	2.832(4)	114(5)
N(1)-H(1)···I(1) ^{# b}	0.81(6)	2.72(6)	3.458(3)	152(5)

^a Numbering scheme in Fig. S13. ^b Symmetry transformation used to generate equivalent atoms:

#: $-x+1, y, -z+1/2$.

Table S18 Summary of Crystal Data, Intensity Measurements and Structure Refinements for $[\text{Zn}(\text{L2})](\text{CF}_3\text{SO}_3)_2$ (**6**).

6	
Empirical formula	$\text{C}_{21}\text{H}_{13}\text{F}_6\text{N}_5\text{O}_6\text{S}_2\text{Zn}$
Formula weight	674.85
Temperature	293(2)K
Wavelength	1.54184 Å
Crystal System, Space group	Triclinic, $P\bar{1}$
Unit cell dimensions	$a = 10.7189(4)$ Å $b = 14.6809(5)$ Å $c = 16.4269(5)$ Å $\alpha = 88.059(3)^\circ$ $\beta = 74.043(3)^\circ$. $\gamma = 89.386(3)^\circ$
Volume in Å ³	2483.96(15)
Z, Calculated density	4, 1.805 Mg/m ³
Absorption coefficient	3.833 mm ⁻¹
$F(000)$	1352
Theta range for data collection	2.80 to 73.22 °
Limiting indices	-13≤ h ≤13, -18≤ k ≤13, -17≤ l ≤20
Reflections collected / unique	18642 / 9705 [$R(\text{int}) = 0.0579$]
Completeness to theta	66.97° / 100%
Data / restraints / parameters	9705 / 18 / 726
Goodness-of-fit on F^2	1.373
Final R indices [$I > 2\sigma(I)$]	$R_1 = 0.0839$, $\omega R_2 = 0.2518$
R indices (all data)	$R_1 = 0.1017$, $\omega R_2 = 0.2784$
Largest diff. peak and hole	3.674 and -1.643 e.Å ⁻³

Table S19 Selected Bond Distances (Å), Bond Angles (°) in [Zn(**L2**)](CF₃SO₃)₂ (**6**).^a

Bond Distances (Å)					
Atom 1	Atom 2	Distance	Atom 1	Atom 2	Distance
Zn(1A)	N(1A)	1.997(4)	Zn(1B)	N(1B)	1.999(4)
Zn(1A)	N(3A)	2.245(4)	Zn(1B)	N(3B)	2.234(4)
Zn(1A)	N(5A)	2.002(4)	Zn(1B)	N(5B)	1.992(4)
Zn(1A)	O(1TB)	1.983(13)	Zn(1B)	O(7T)	2.038(4)
Zn(1A)	O(1TA)	2.087(12)	Zn(1B)	O(10T)	2.114(4)
Zn(1A)	O(4)	2.114(4)			

Angles (°)							
Atom 1	Atom 2	Atom 3	Angle	Atom 1	Atom 2	Atom 3	Angle
O(1TB)	Zn(1A)	N(1A)	113.2(4)	N(5B)	Zn(1B)	N(1B)	127.06(17)
O(1TB)	Zn(1A)	N(5A)	115.9(4)	N(5B)	Zn(1B)	O(7T)	127.68(19)
N(1A)	Zn(1A)	N(5A)	128.72(17)	N(1B)	Zn(1B)	O(7T)	104.35(18)
O(1TB)	Zn(1A)	O(1TA)	14.5(4)	N(5B)	Zn(1B)	O(10T)	94.79(19)
N(1A)	Zn(1A)	O(1TA)	101.7(3)	N(1B)	Zn(1B)	O(10T)	95.29(18)
N(5A)	Zn(1A)	O(1TA)	129.0(3)	O(7T)	Zn(1B)	O(10T)	88.93(19)
O(1TB)	Zn(1A)	O(4T)	94.3(4)	N(5B)	Zn(1B)	N(3B)	89.68(17)
N(1A)	Zn(1A)	O(4T)	95.75(17)	N(1B)	Zn(1B)	N(3B)	87.70(17)
N(5A)	Zn(1A)	O(4T)	94.68(17)	O(7T)	Zn(1B)	N(3B)	82.66(18)
O(1TA)	Zn(1A)	O(4T)	86.8(3)	O(10T)	Zn(1B)	N(3B)	171.53(18)
O(1TB)	Zn(1A)	N(3A)	77.8(4)				
N(1A)	Zn(1A)	N(3A)	89.82(17)				
N(5A)	Zn(1A)	N(3A)	86.58(16)				
O(1TA)	Zn(1A)	N(3A)	86.1(3)				
O(4T)	Zn(1A)	N(3A)	171.68(18)				

^a Numbering scheme in Fig. 7

Table S20 Selected Least-Squares Planes Data for [Zn(**L2**)](CF₃SO₃)₂ (**6**).^a

Least-Squares Planes			
Least-squares planes description	Abbreviation	Max. deviation/Å	Atom
Azaindole 1a C1a C2a C3a C4a C5a C6a N2a C7a N1a	Az1a	0.02(1)	C5a
Pyridine a N3a C8a C9a C10a C11a C12a	Pya	0.02(1)	C8a
Azaindole 2a C13a C14a C15a C16a C17a C18a N5a C19a N4a	Az2a	0.04(1)	N5a
Azaindole 1b C1a C2a C3a C4a C5a C6a N2a C7a N1a	Az1b	0.03(1)	C5b
Pyridine b N3a C8a C9a C10a C11a C12a	Pyb	0.03(1)	N3b
Azaindole 2b C13a C14a C15a C16a C17a C18a N5a C19a N4a	Az2b	0.02(1)	C16b

^a Numbering scheme in Fig. S7

Interplanar angles (°) (esd < 0.1°)

	Pya	Az2a
Az1a	27.9	44.0
Pya		26.8

	Pyb	Az2b
Az1b	25.2	44.6
Pyb		28.2

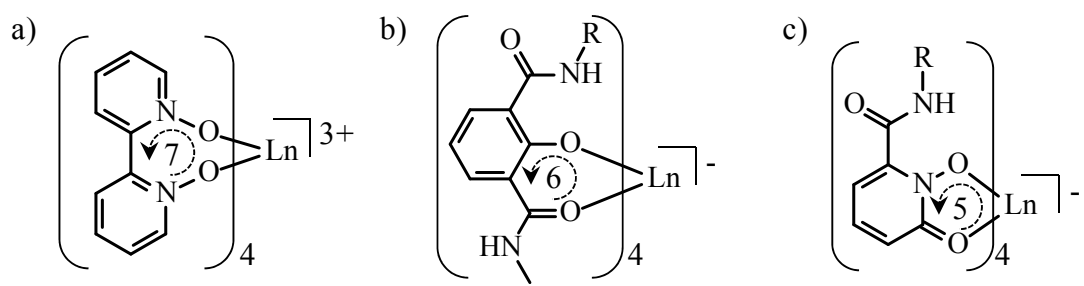


Figure S1 Selected stable lanthanide complexes with a) seven-membered^{2c}, b) six-membered^{3c} and c) five-membered^{4c} aromatic chelate rings.

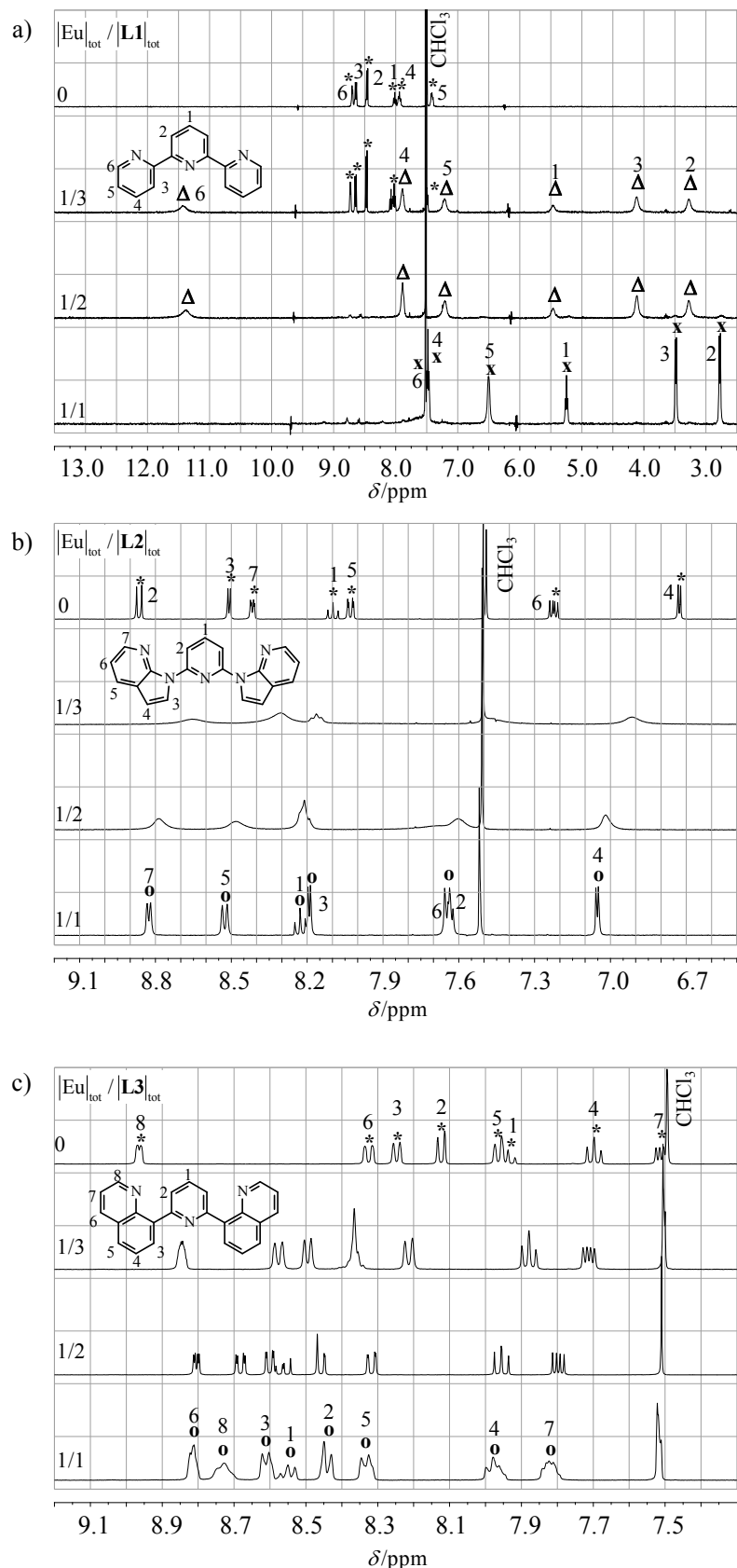


Figure S2 ^1H NMR titrations of a) **L1**, b) **L2** and c) **L3** with $\text{Eu}(\text{CF}_3\text{SO}_3)_3 \cdot \text{H}_2\text{O}$ in $\text{CD}_3\text{CN}/\text{CDCl}_3$ (1:1) at 298 K ($[\text{Lk}]_{\text{tot}} = 7.5 \cdot 10^{-3}$ M). Codes: * = **Lk**, o = $[\text{HLk}]^+$, x = $[\text{Eu(Lk)}]^{3+}$, Δ = $[\text{Eu(Lk)}_2]^{3+}$.

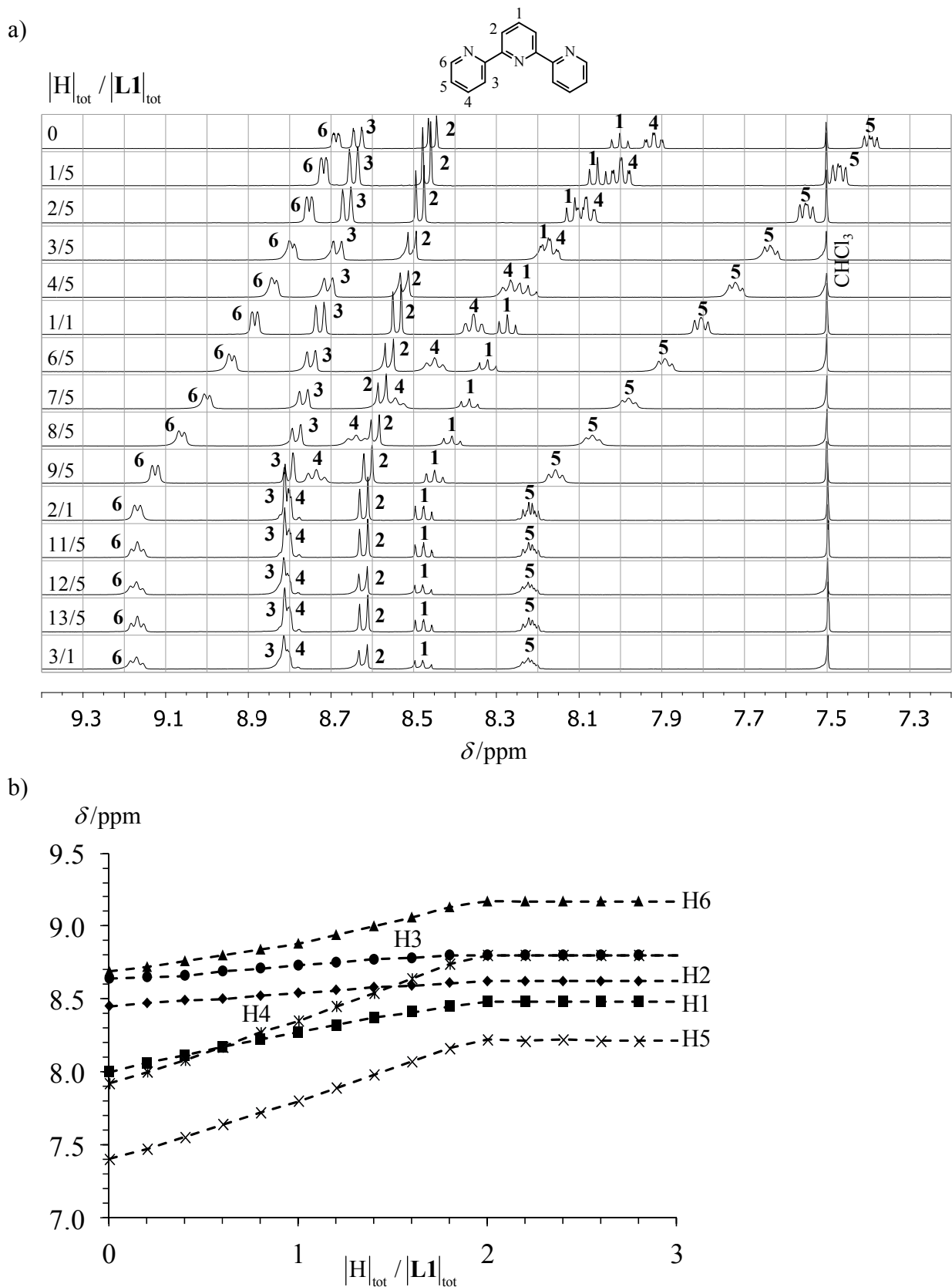


Figure S3 Variation of a) ^1H NMR spectra and b) ^1H NMR chemical shifts for the titration of **L1** with $\text{CF}_3\text{SO}_3\text{H}$ in $\text{CD}_3\text{CN}/\text{CDCl}_3$ (1:1) (total ligand concentration 7.5 mM, 298 K).

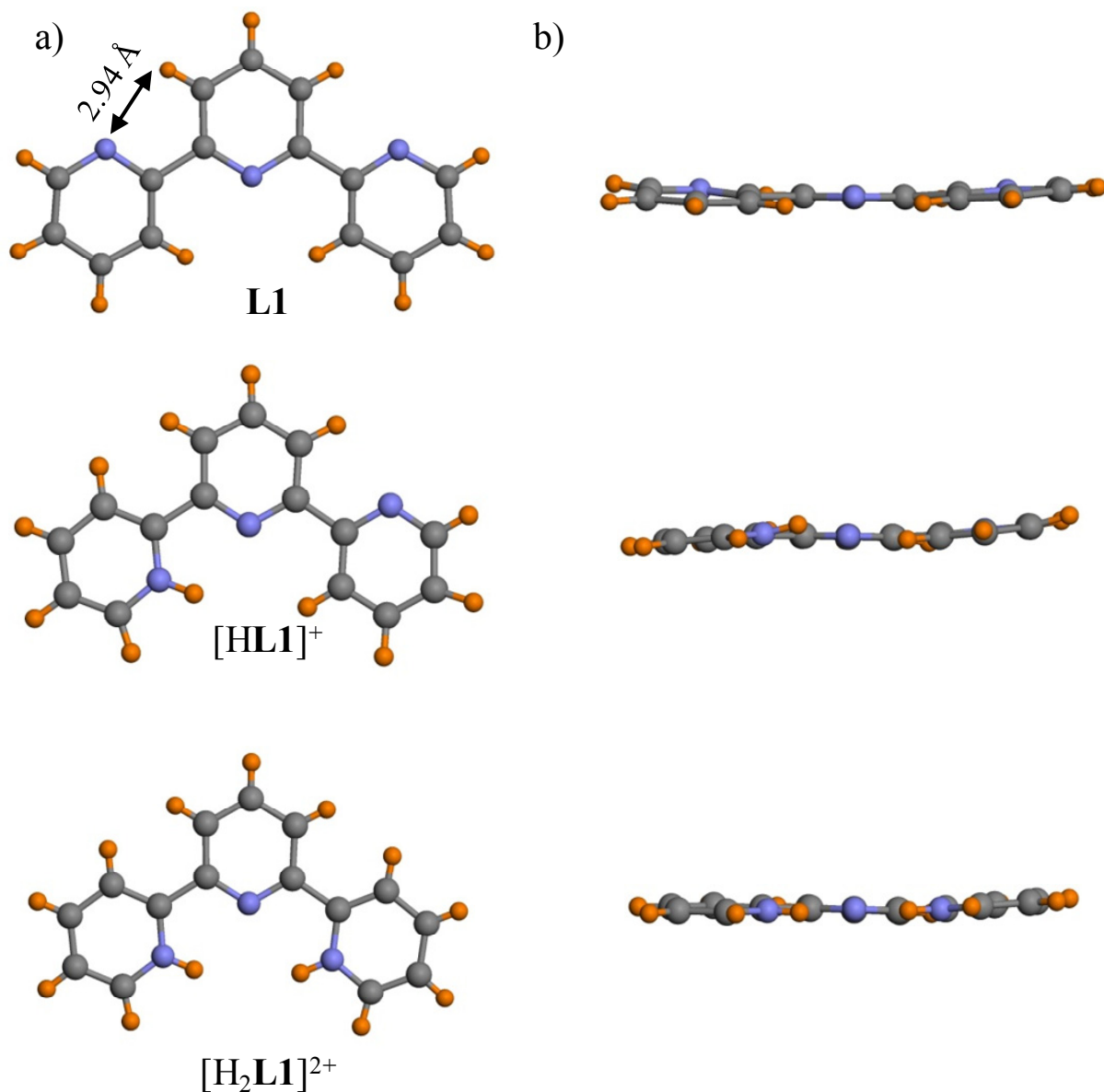


Figure S4 Perspective views a) perpendicular and b) parallel to the central pyridine ring of the molecular structures of **L1**, $[\text{HL1}]^+$, $[\text{H}_2\text{L1}]^{2+}$ observed in the crystal structures of **L1**,^{18b} $[\text{HL1}](\text{CF}_3\text{SO}_3)$,²⁰ and $[\text{H}_2\text{L1}](\text{NO}_3)_2$.^{21c} Redrawn from the original CIF files. Color code: grey = C, blue = N, orange = H.

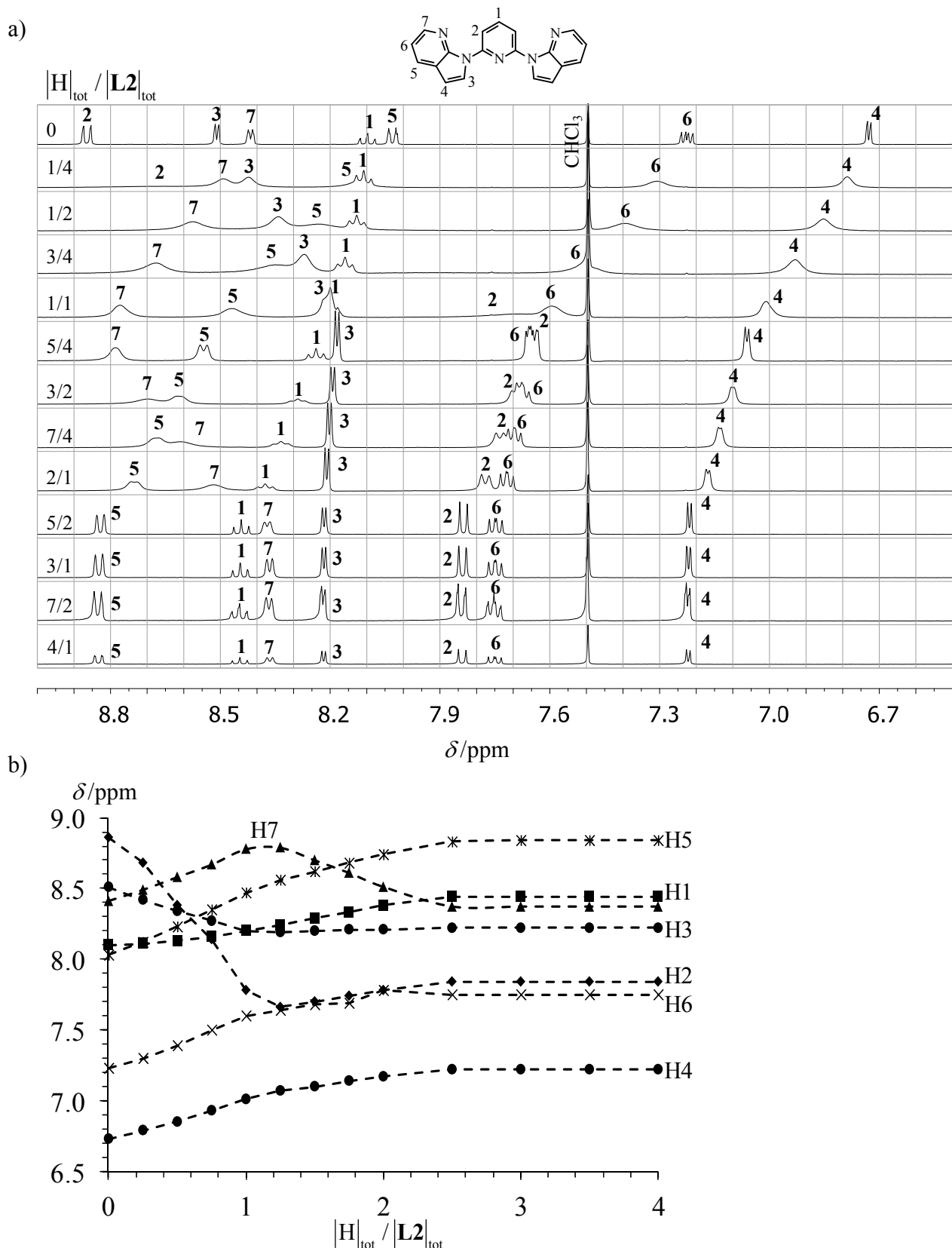


Figure S5 Variation of a) ^1H NMR spectra and b) ^1H NMR chemical shifts for the titration of **L2** with $\text{CF}_3\text{SO}_3\text{H}$ in $\text{CD}_3\text{CN}/\text{CDCl}_3$ (1:1) (total ligand concentration 7.5 mM, 298 K).

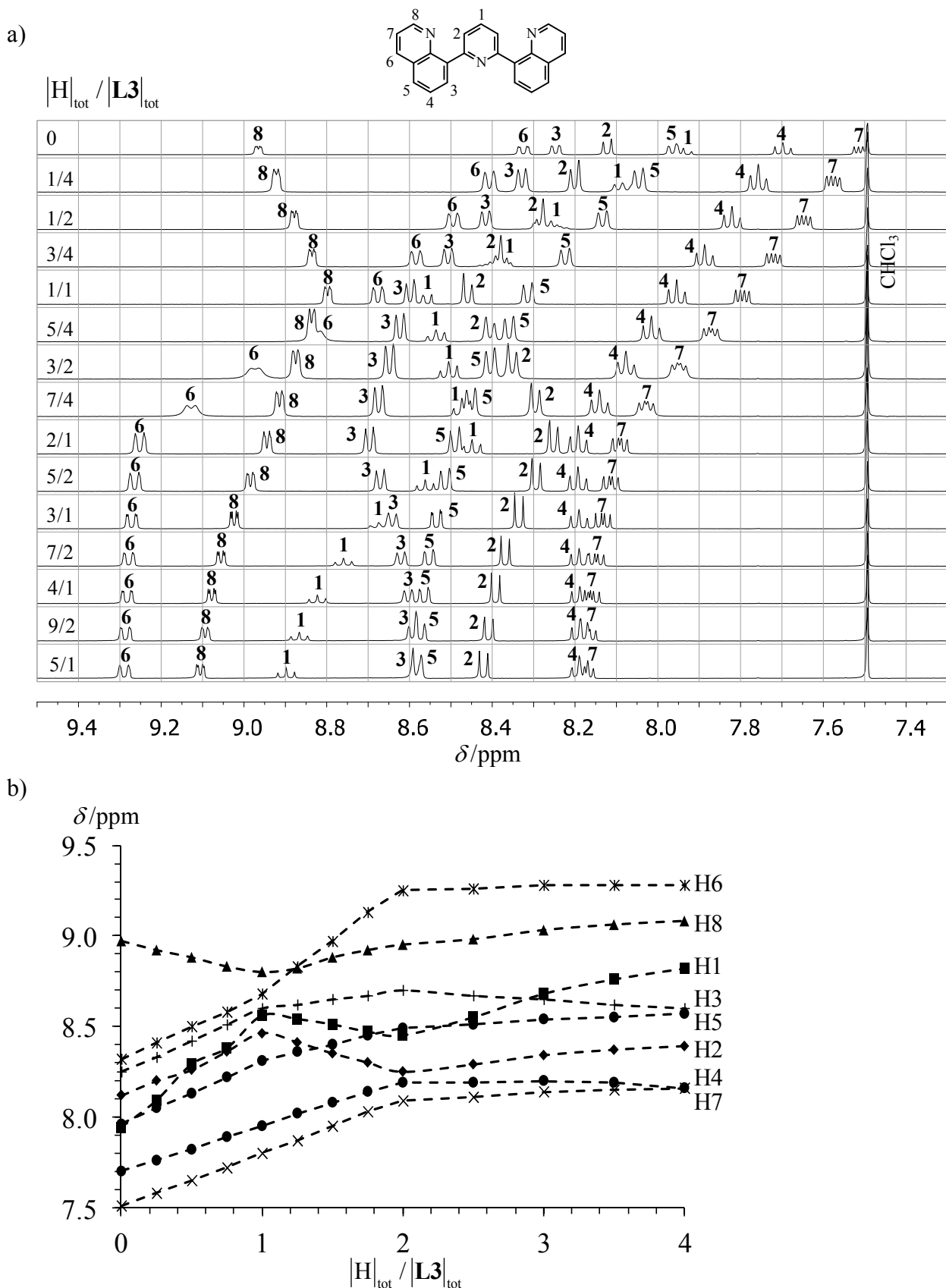


Figure S6 Variation of a) ^1H NMR spectra and b) ^1H NMR chemical shifts for the titration of **L3** with CF₃SO₃H in CD₃CN/CDCl₃ (1:1) (total ligand concentration 7.5 mM, 298 K).

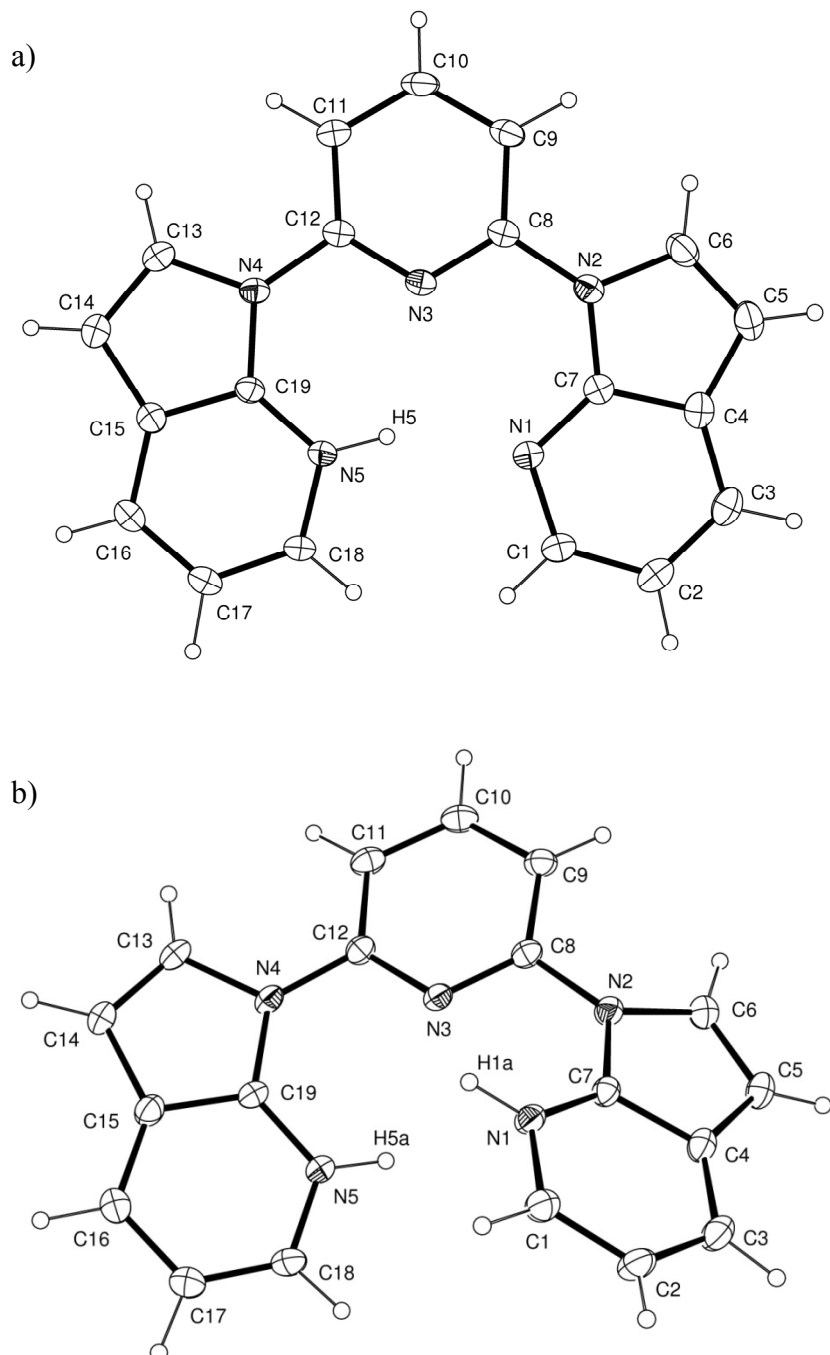


Figure S7 ORTEP views of a) $[\text{HL2}]^+$ and b) $[\text{H}_2\text{L2}]^{2+}$ observed in the crystal structures of $[\text{HL2}](\text{CF}_3\text{SO}_3)$ (**1**) and $[\text{H}_2\text{L2}](\text{CF}_3\text{SO}_3)_2$ (**2**) with atomic numbering scheme. Thermal ellipsoids are represented at the 50% probability level.

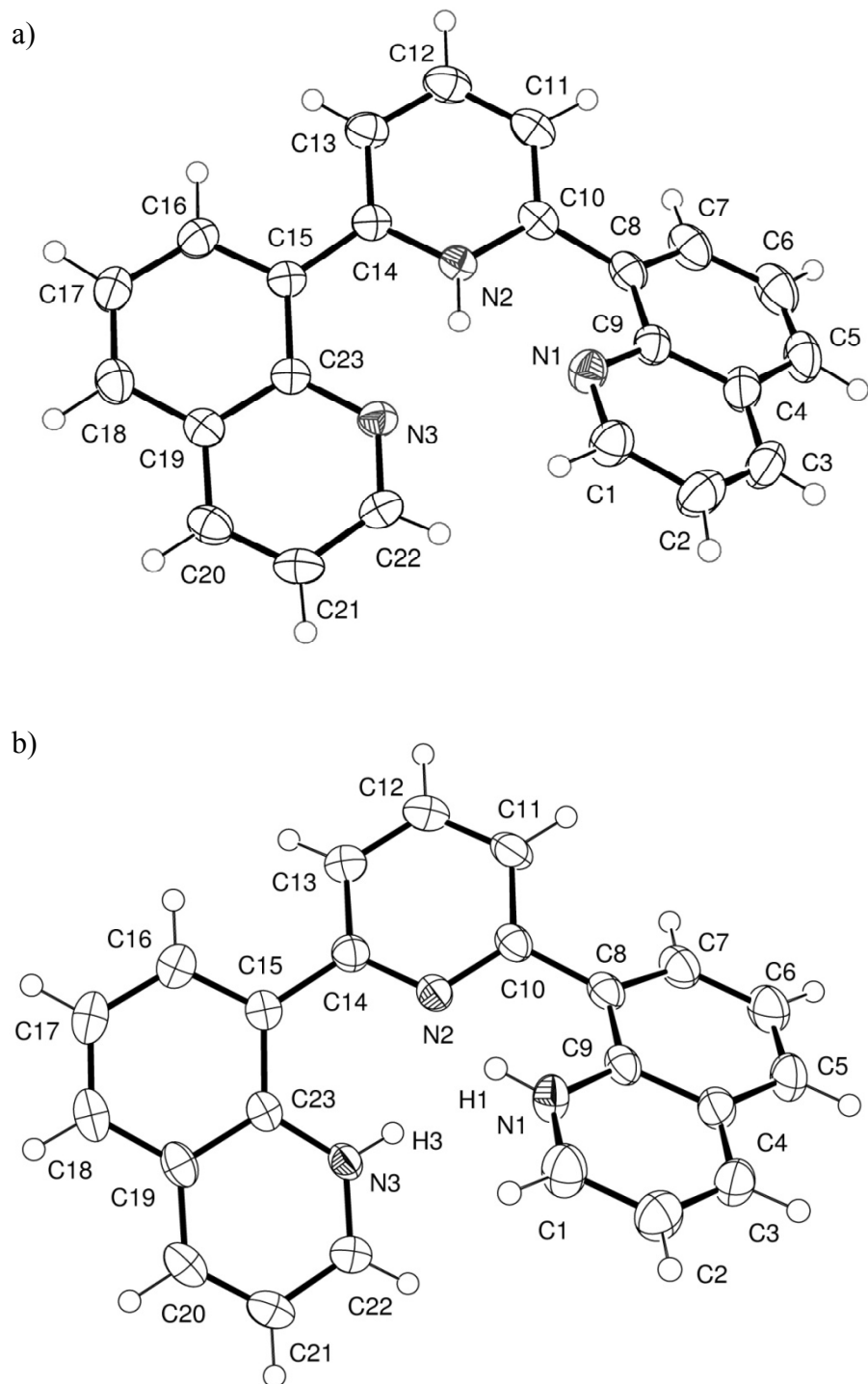


Figure S8 ORTEP views of a) $[\text{HL3}]^+$ and b) $[\text{H}_2\text{L3}]^{2+}$ observed in the crystal structures of $[\text{HL3}](\text{CF}_3\text{SO}_3)$ (**3**) and $[\text{H}_2\text{L3}](\text{CF}_3\text{SO}_3)_2$ (**4**) with atomic numbering scheme. Thermal ellipsoids are represented at the 50% probability level.

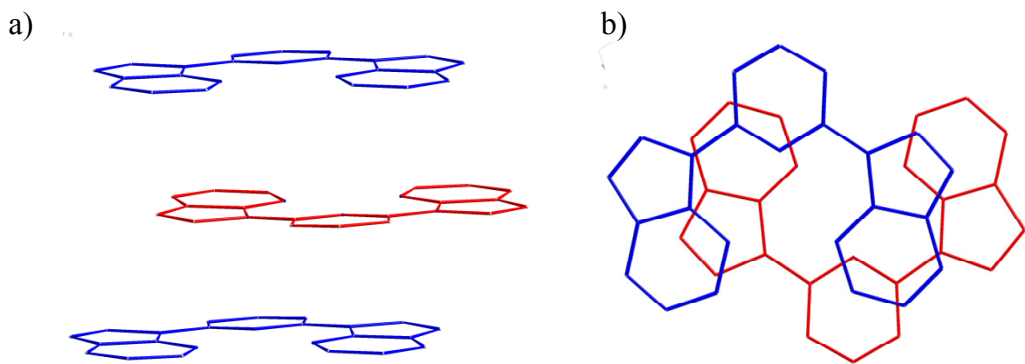


Figure S9 View of intermolecular π -stacking interactions for $[\text{HL2}]^+$ cations related by inversion centers in the crystal structure of $[\text{HL2}](\text{CF}_3\text{SO}_3)$ (**1**) a) down to the b axis (interplanar distance = 3.3 Å) and b) along the b axis showing the minor inter-aromatic overlap.

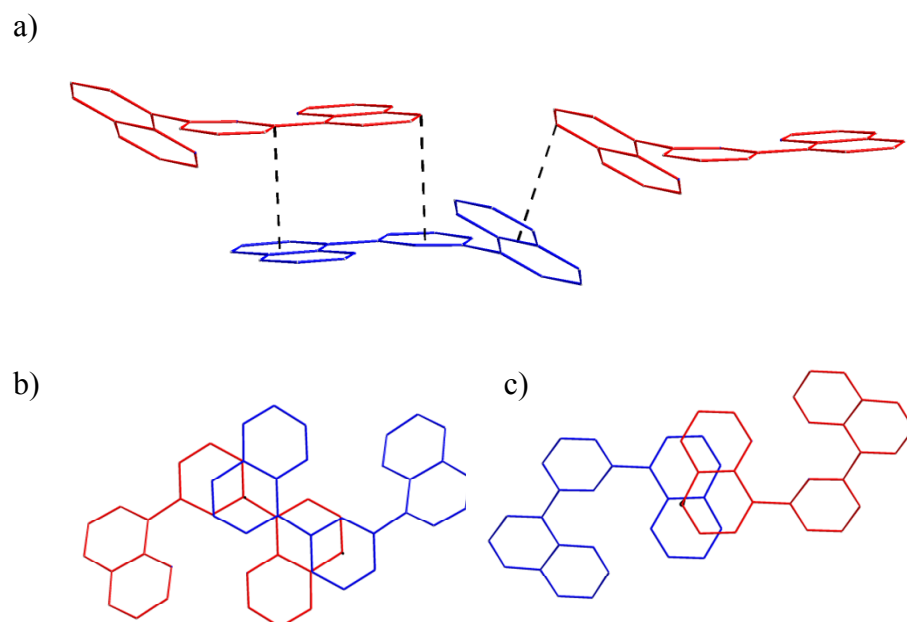


Figure S10 View of intermolecular π -stacking interactions for $[\text{HL3}]^+$ cations related by inversion centers in the crystal structure of $[\text{HL3}](\text{CF}_3\text{SO}_3)$ (**3**) a) perpendicular to the packing direction (dotted black lines are only guides for the eyes) and b,c) along the packing direction showing the minor inter-aromatic overlap (b) $d_{\text{quinoline}}-d_{\text{pyridine}} = 3.5 \text{ \AA}$, $d_{\text{pyridine}}-d_{\text{quinoline}} = 3.3 \text{ \AA}$ and c) $d_{\text{quinoline}}-d_{\text{quinoline}} = 3.4 \text{ \AA}$.

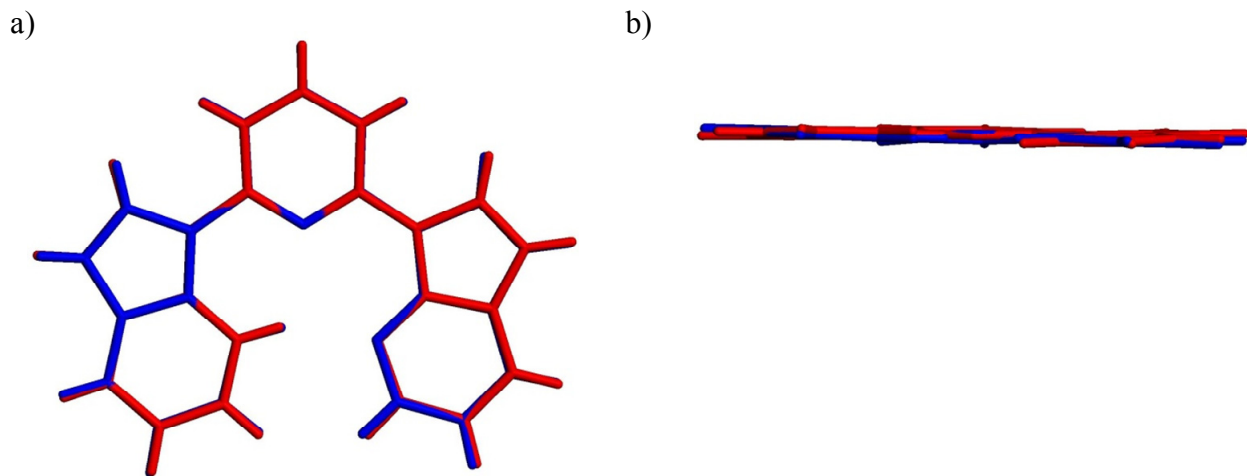


Figure S11 Superimposed perspective views a) perpendicular and b) parallel to the central pyridine ring of the molecular structures of $[HL2]^{2+}$ observed in the crystal structures of $[HL2](CF_3SO_3)$ (blue) and $[HL2](FeCl_4)^{10}$ (red).

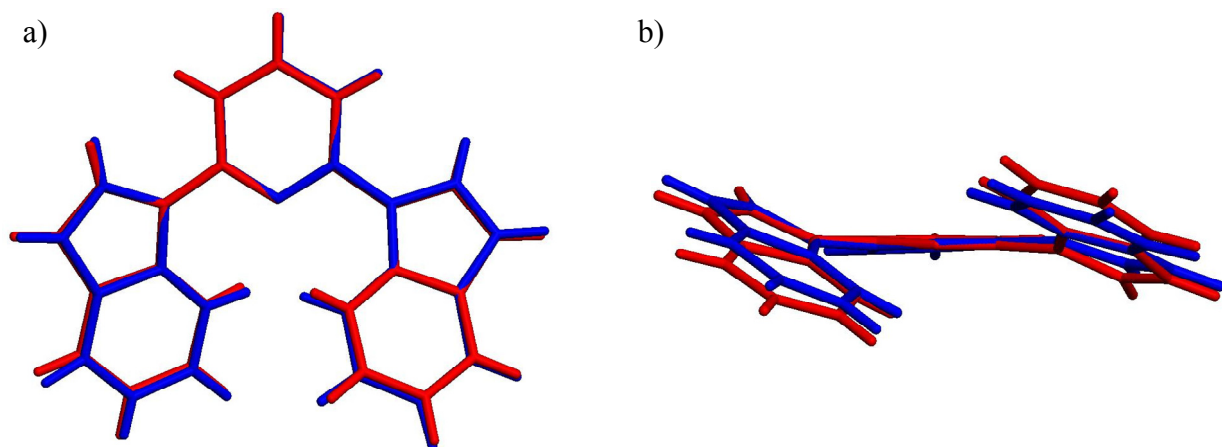


Figure S12 Superimposed perspective views a) perpendicular and b) parallel to the central pyridine ring of the molecular structures of $[H_2L2]^{2+}$ observed in the crystal structures of $[H_2L2](CF_3SO_3)_2$ (blue) and $[H_2L2]I_2$ (red).

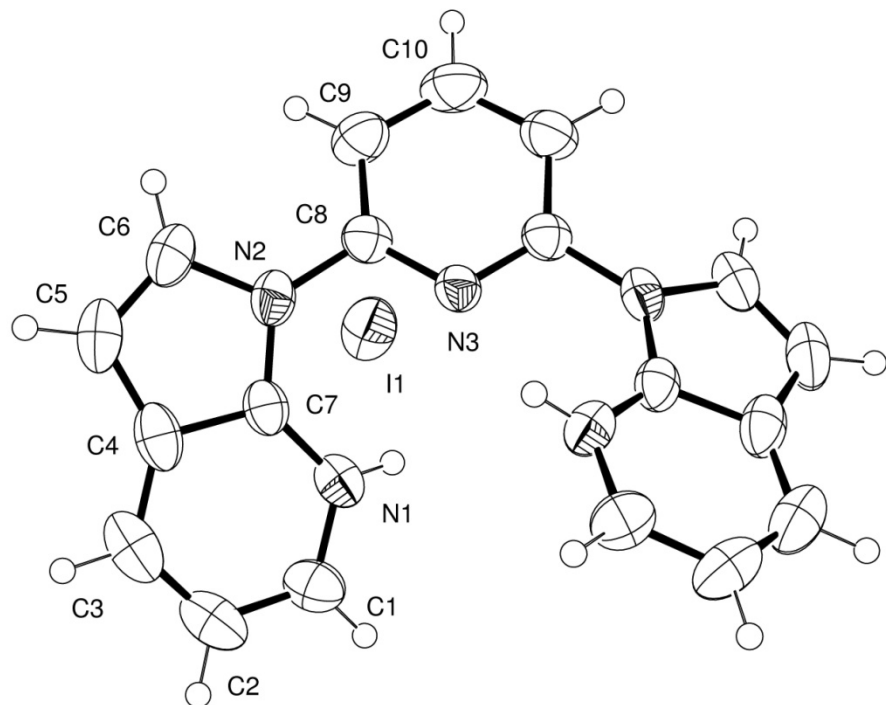
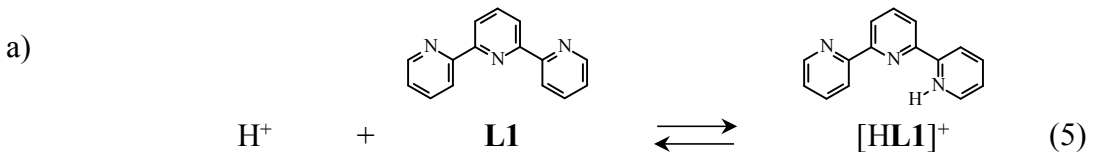


Figure S13 ORTEP views of a) $[H_2\mathbf{L}2]^+$ observed in the crystal structures of $[H_2\mathbf{L}2]I_2$ (**5**) with atomic numbering scheme. Thermal ellipsoids are represented at the 50% probability level.



Point groups: R_3 C_{2v} $\beta_{1,1}^{\text{H,L1}}(\text{distal})$ C_s

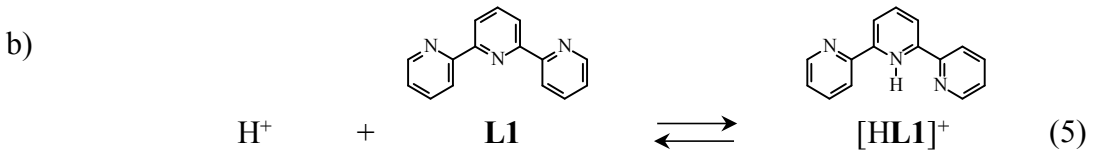
$$\sigma^{\text{ext}}: \quad 1 \quad 2 \quad 1$$

$$\sigma^{\text{int}}: \quad 1 \quad 1 \quad 1$$

$$\sigma^{\text{chiral}}: \quad 1 \quad 1 \quad 1$$

$$\omega_{1,1}^{\text{H,L1}}(\text{distal}) = \frac{(\sigma_{\text{H}}^{\text{ext}} \sigma_{\text{H}}^{\text{int}} \sigma_{\text{H}}^{\text{chiral}}) \cdot (\sigma_{\text{L1}}^{\text{ext}} \sigma_{\text{L1}}^{\text{int}} \sigma_{\text{L1}}^{\text{chiral}})}{(\sigma_{\text{HL1}}^{\text{ext}} \sigma_{\text{HL1}}^{\text{ext}} \sigma_{\text{HL1}}^{\text{chiral}})} = 2$$

$$\Rightarrow \beta_{1,1}^{\text{H,L1}}(\text{distal}) = \omega_{1,1}^{\text{H,L1}}(\text{distal}) f_{\text{distal}}^{\text{H,L1}} = 3 f_{\text{distal}}^{\text{H,L1}}$$



Point groups: R_3 C_{2v} $\beta_{1,1}^{\text{H,L1}}(\text{central})$ C_{2v}

$$\sigma^{\text{ext}}: \quad 1 \quad 2 \quad 2$$

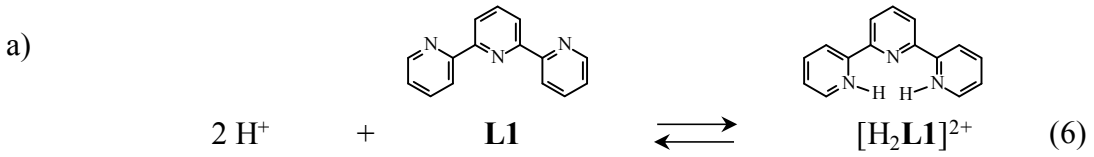
$$\sigma^{\text{int}}: \quad 1 \quad 1 \quad 1$$

$$\sigma^{\text{chiral}}: \quad 1 \quad 1 \quad 1$$

$$\omega_{1,1}^{\text{H,L1}}(\text{central}) = \frac{(\sigma_{\text{H}}^{\text{ext}} \sigma_{\text{H}}^{\text{int}} \sigma_{\text{H}}^{\text{chiral}}) \cdot (\sigma_{\text{L1}}^{\text{ext}} \sigma_{\text{L1}}^{\text{int}} \sigma_{\text{L1}}^{\text{chiral}})}{(\sigma_{\text{HL1}}^{\text{ext}} \sigma_{\text{HL1}}^{\text{ext}} \sigma_{\text{HL1}}^{\text{chiral}})} = 1$$

$$\Rightarrow \beta_{1,1}^{\text{H,L1}}(\text{central}) = \omega_{1,1}^{\text{H,L1}}(\text{central}) f_{\text{central}}^{\text{H,L1}} = f_{\text{central}}^{\text{H,L1}}$$

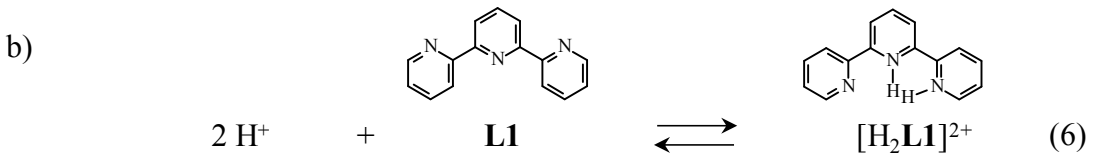
Figure S14 Application of the site binding model²⁶ showing the determination of symmetry numbers (σ^{ext} , σ^{int} , σ^{chiral})²⁷ for the two microspecies contributing to equilibrium (5). The symmetry point groups are those expected for coplanar arrangements of the pyridine rings.



Point groups:	R_3	C_{2v}	$\beta_{2,1}^{\text{H,L1}}(\text{distal})$	C_{2v}
σ^{ext} :	1	2		2
σ^{int} :	1	1		1
σ^{chiral} :	1	1		1

$$\omega_{2,1}^{\text{H,L1}}(\text{distal}) = \frac{(\sigma_{\text{H}}^{\text{ext}} \sigma_{\text{H}}^{\text{int}} \sigma_{\text{H}}^{\text{chiral}})^2 \cdot (\sigma_{\text{L1}}^{\text{ext}} \sigma_{\text{L1}}^{\text{int}} \sigma_{\text{L1}}^{\text{chiral}})}{(\sigma_{\text{H2L1}}^{\text{ext}} \sigma_{\text{H2L1}}^{\text{ext}} \sigma_{\text{H2L1}}^{\text{chiral}})} = 1$$

$$\Rightarrow \beta_{2,1}^{\text{H,L1}}(\text{distal}) = \omega_{2,1}^{\text{H,L1}}(\text{distal}) (f_{\text{distal}}^{\text{H,L1}})^2 u_{\text{d,d,L1}}^{\text{H,H}} = (f_{\text{distal}}^{\text{H,L1}})^2 u_{\text{d,d,L1}}^{\text{H,H}}$$



Point groups:	R_3	C_{2v}	$\beta_{2,1}^{\text{H,L1}}(\text{central})$	C_s
σ^{ext} :	1	2		1
σ^{int} :	1	1		1
σ^{chiral} :	1	1		1

$$\omega_{2,1}^{\text{H,L1}}(\text{central}) = \frac{(\sigma_{\text{H}}^{\text{ext}} \sigma_{\text{H}}^{\text{int}} \sigma_{\text{H}}^{\text{chiral}})^2 \cdot (\sigma_{\text{L1}}^{\text{ext}} \sigma_{\text{L1}}^{\text{int}} \sigma_{\text{L1}}^{\text{chiral}})}{(\sigma_{\text{H2L1}}^{\text{ext}} \sigma_{\text{H2L1}}^{\text{ext}} \sigma_{\text{H2L1}}^{\text{chiral}})} = 2$$

$$\Rightarrow \beta_{2,1}^{\text{H,L1}}(\text{central}) = \omega_{2,1}^{\text{H,L1}}(\text{central}) (f_{\text{central}}^{\text{H,L1}}) (f_{\text{distal}}^{\text{H,L1}}) u_{\text{c,d,L1}}^{\text{H,H}} = 2 (f_{\text{central}}^{\text{H,L1}}) (f_{\text{distal}}^{\text{H,L1}}) u_{\text{c,d,L1}}^{\text{H,H}}$$

Figure S15 Application of the site binding model²⁶ showing the determination of symmetry numbers (σ^{ext} , σ^{int} , σ^{chiral})²⁷ for the two microspecies contributing to equilibrium (6). The symmetry point groups are those expected for coplanar arrangements of the pyridine rings.

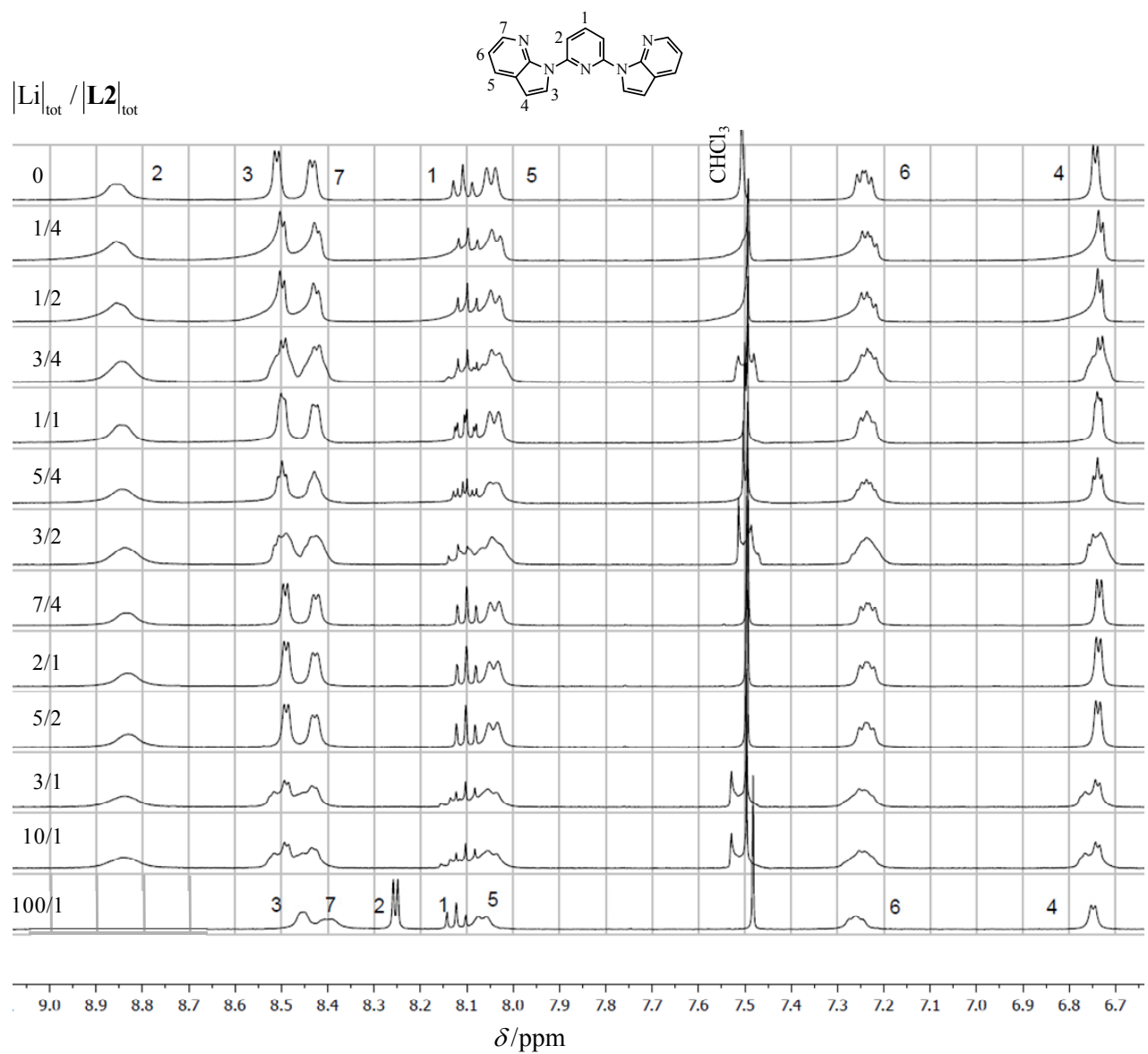


Figure S16 Variation of ^1H NMR spectra for the titration of **L2** with LiClO_4 in $\text{CD}_3\text{CN}/\text{CDCl}_3$ (1:1) (total ligand concentration 7.5 mM, 298 K).

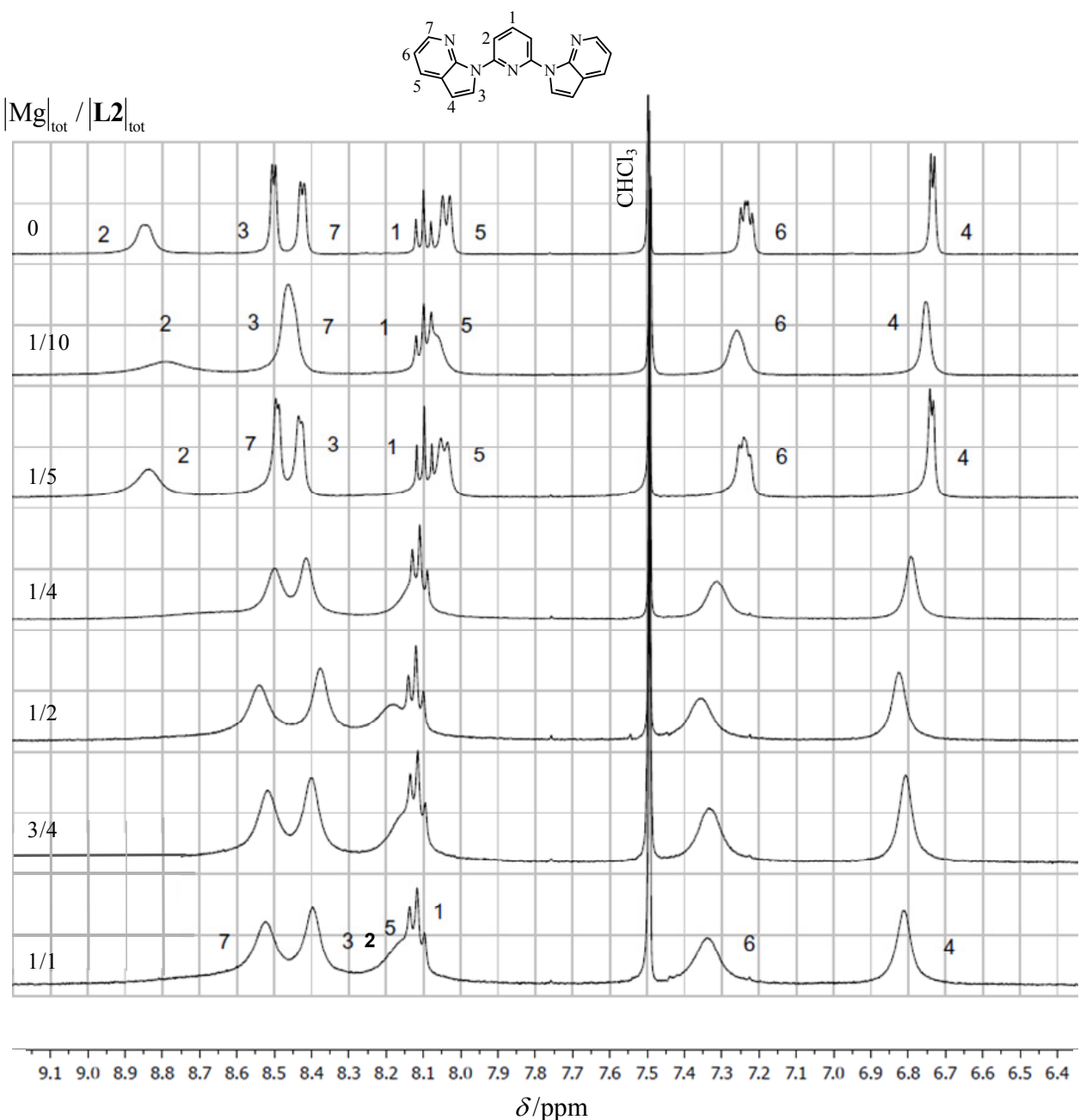


Figure S17 Variation of ^1H NMR spectra for the titration of **L2** with $\text{Mg}(\text{ClO}_4)_2$ in $\text{CD}_3\text{CN}/\text{CDCl}_3$ (1:1) (total ligand concentration 7.5 mM, 298 K).

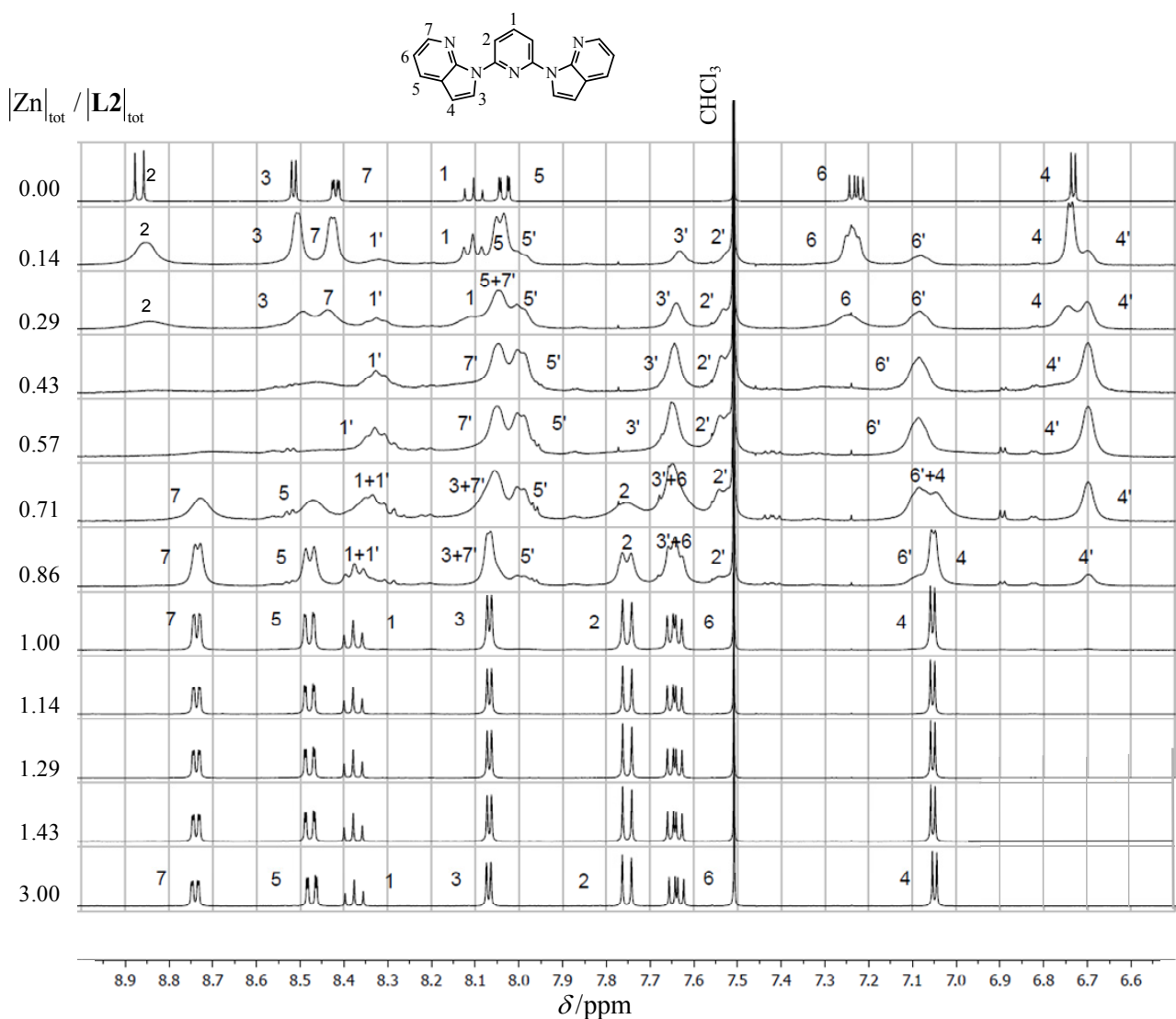


Figure S18 Variation of ^1H NMR spectra for the titration of **L2** with $\text{Zn}(\text{CF}_3\text{SO}_3)_2$ in $\text{CD}_3\text{CN}/\text{CDCl}_3$ (1:1) (total ligand concentration 7.5 mM, 298 K). Numbering scheme: unprimed = $[\text{Zn}(\text{L2})]^{2+}$, primed = $[\text{Zn}(\text{L2}_2)]^{2+}$, double-primed = **L2**.

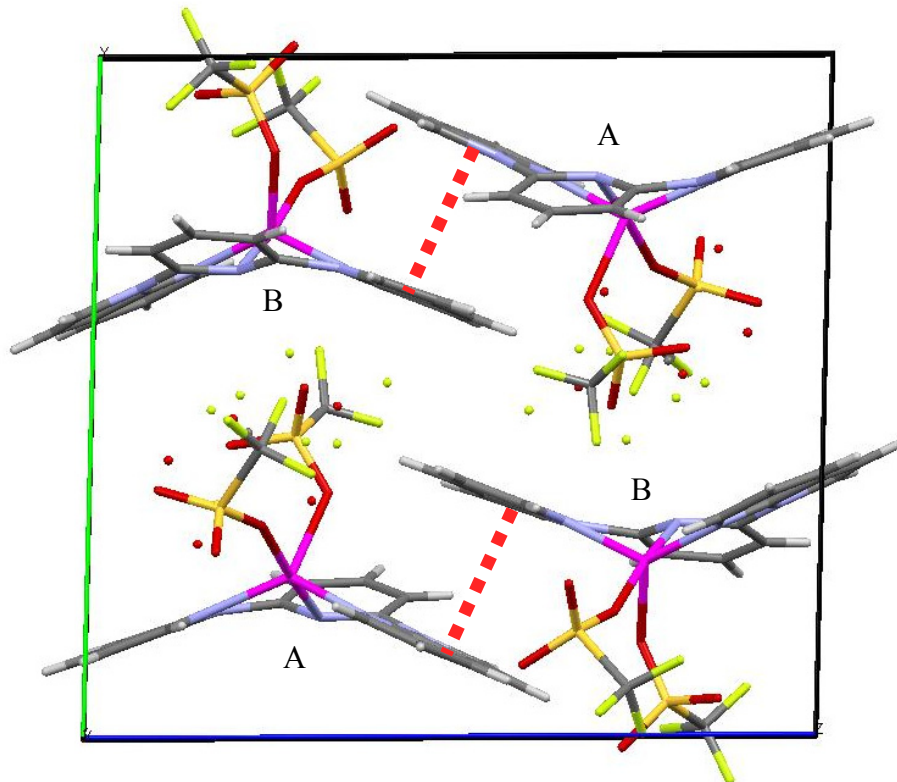


Figure S19 Crystal packing in $\text{Zn}(\text{L2})(\text{CF}_3\text{SO}_3)_2$ (**6**) viewed along the a axis. Intermolecular π -stacking interactions are shown in red (dashed line, $d = 3.6 \text{ \AA}$, interplanar angle = 5.1°). The colored dots in the molecular structure of A- $\text{Zn}(\text{L2})(\text{CF}_3\text{SO}_3)_2$ show the positions of the oxygen and fluoride atoms of the triflate couter-anions in the minor conformer.

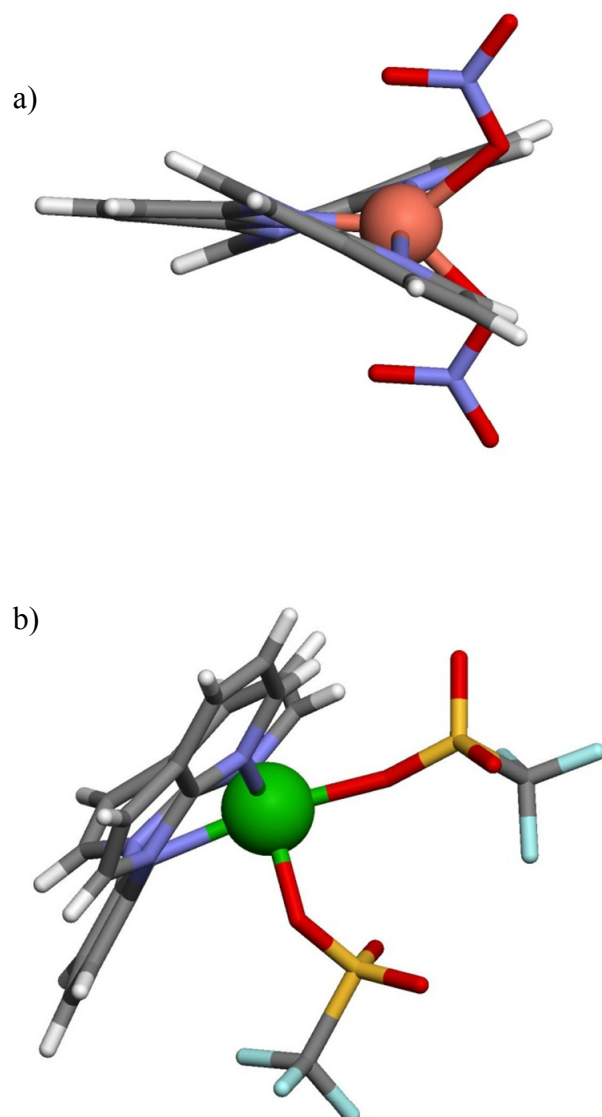
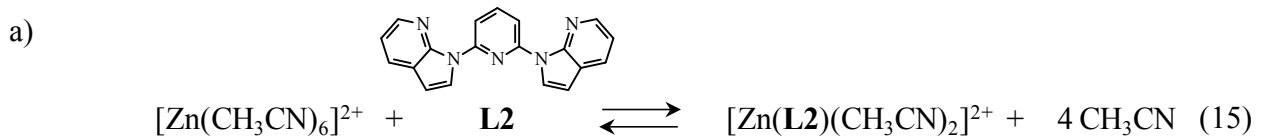


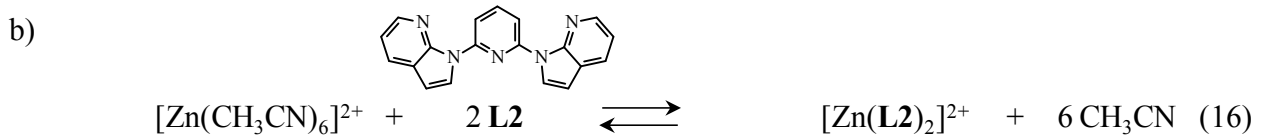
Figure S20 Perspective views the molecular structures of the meridionally ter-coordinated 2,6-(bis(azaindol-yl)pyridine ligand in a) $[\text{Cu}(\text{L2})](\text{NO}_3)_2$ (twisted conformation)¹⁰ and b) $[\text{Zn}(\text{L2})](\text{CF}_3\text{SO}_3)_2$ (butterfly conformation). Color code: H = white, C = grey, N = dark blue, O = red, F = light blue, S = yellow, Cu = salmon, Zn = green.



Point groups:	O_h	C_{2v}	$\beta_{1,1}^{\text{Zn,L2}}$	C_s	C_{3v}
$\sigma^{\text{ext.}}$:	24	2		1	3
$\sigma^{\text{int.}}$:	3^6	1		3^2	1
$\sigma^{\text{chiral.}}$:	1	1		1	1

$$\omega_{1,1}^{\text{Zn,L2}} = \frac{(24 \cdot 3^6 \cdot 1) \cdot (2 \cdot 1 \cdot 1)}{(1 \cdot 3^2 \cdot 1) \cdot (3 \cdot 1 \cdot 1)^4} = 48$$

$$\Rightarrow \beta_{1,1}^{\text{Zn,L2}} = \omega_{1,1}^{\text{Zn,L2}} (f_{\text{connect}}^{\text{Zn,L2}}) = 48 (f_{\text{connect}}^{\text{Zn,L2}}) \quad (17)$$



Point groups:	O_h	C_{2v}	$\beta_{1,1}^{\text{Zn,L2}}$	D_{2d}	C_{3v}
$\sigma^{\text{ext.}}$:	24	2		4	3
$\sigma^{\text{int.}}$:	3^6	1		1	1
$\sigma^{\text{chiral.}}$:	1	1		1	1

$$\omega_{1,2}^{\text{Zn,L2}} = \frac{(24 \cdot 3^6 \cdot 1) \cdot (2 \cdot 1 \cdot 1)^2}{(4 \cdot 1 \cdot 1) \cdot (3 \cdot 1 \cdot 1)^6} = 24$$

$$\Rightarrow \beta_{1,2}^{\text{Zn,L2}} = \omega_{1,2}^{\text{Zn,L2}} (f_{\text{connect}}^{\text{Zn,L2}})^2 u_{\text{Zn}}^{\text{L2,L2}} = 24 (f_{\text{connect}}^{\text{Zn,L2}})^2 u_{\text{Zn}}^{\text{L2,L2}} \quad (18)$$

Figure S21 Application of the site binding model²⁶ showing the determination of symmetry numbers ($\sigma^{\text{ext.}}$, $\sigma^{\text{int.}}$, $\sigma^{\text{chiral.}}$)²⁷ for the microspecies contributing to equilibria (15)-(16). The symmetry point groups are those expected for average five-coordinate $[\text{Zn}(\text{L2})]^{2+}$ and six-coordinate $[\text{Zn}(\text{L2})_2]^{2+}$ complexes in solution.